Biochemistry and Chemical Biology

Optogenetic control of Protein Kinase C-epsilon activity reveals its intrinsic signaling properties with spatiotemporal resolution

Reviewed Preprint
v1 • March 24, 2025
Not revised

Qunxiang Ong, Crystal Jing Yi Lim, Yilie Liao, Justin Tze-Yang Ng, Ler Ting Rachel Lim, Shernys Xuan Yi Koh, Sher En Chan, Pheobe Lee Yu Ying, Huijun Lim, Chen Rui Ye, Loo Chien Wang, Siok Ghee Ler, Radoslaw M Sobota, Yaw Sing Tan, Gerald I Shulman, Xiaoyong Yang, Weiping Han

Laboratory of Metabolic Medicine, Institute of Molecular and Cell Biology, Agency for Science, Technology and Research (A*STAR), Singapore, Singapore • Duke-NUS Medical School, National University of Singapore, Singapore, Singapore • Bioinformatics Institute, Agency for Science, Technology and Research (A*STAR), Singapore, Singapore • Functional Proteomics Laboratory, SingMass National Laboratory, Institute of Molecular and Cell Biology, Agency for Science, Technology and Research (A*STAR), Singapore, Singapore • Departments of Internal Medicine and Cellular & Molecular Physiology, Yale School of Medicine, New Haven, United States • Howard Hughes Medical Institute, Chevy Chase, United States • Departments of Comparative Medicine and Cellular & Molecular Physiology, Yale School of Medicine, New Haven, United States

eLife Assessment

This manuscript introduces Opto-PKCε, an optogenetic tool that enabled **important** findings derived from interactome and phosphoproteome studies. Light-dependent recruitment of Opto-PKCε to the plasma membrane revealed the specific phosphorylation of the insulin receptor at Thr 1160. In turn, recruitment to mitochondria led to phosphorylation of the complex I subunit NDUFS4, correlating with reduced spare respiratory capacity. The evidence supporting these conclusions is **solid**, although additional clarification on data analysis would further enhance readability.

https://doi.org/10.7554/eLife.105796.1.sa2

Abstract

The regulation of PKC epsilon (PKCε) and its downstream effects is still not fully understood, making it challenging to develop targeted therapies or interventions. A more precise tool that enables spatiotemporal control of PKCε activity is thus required. Here, we describe a photo-activatable optogenetic PKCε probe (Opto-PKCε) consisting of an engineered PKCε catalytic domain and a blue-light inducible dimerization domain. Molecular dynamics and AlphaFold simulations enable rationalization of the dark-light activity of the optogenetic probe. We first characterize the binding partners of Opto-PKCε, which are similar to those of PKCε. Subsequent validation of the Opto-PKCε tool is performed with phosphoproteome analysis, which reveals that only PKCε substrates are phosphorylated upon light activation. Opto-PKCε

could be engineered for recruitment to specific subcellular locations. Activation of Opto-PKCε in isolated hepatocytes reveals its sustained activation at the plasma membrane is required for its phosphorylation of the insulin receptor at Thr1160. In addition, Opto-PKCε recruitment to the mitochondria results in its lowering of the spare respiratory capacity through phosphorylation of complex I NDUFS4. These results demonstrate that Opto-PKCε may have broad applications for the studies of PKCε signaling with high specificity and spatiotemporal resolution.

Summary

We have developed a photo-activatable optogenetic PKCε probe, which demonstrates differential activity in light *versus* dark. The tool is subsequently validated with protein association studies and phosphoproteome analysis. It enables dissection of signaling events arising from its activation at defined subcellular locations. For instance, sustained activation of PKCε at the plasma membrane is required for its phosphorylation of the insulin receptor at Thr1160.

Introduction

PKCε is highly expressed in many cell types and involved in a diverse range of cellular processes, including cell proliferation, glucose metabolism, secretion, and memory formation. Consequently, dysfunctional PKCε activity is implicated in the pathogenesis of many diseases, including insulin resistance, type 2 diabetes and neurodegenerative diseases. PKCε is often linked to the formation of Aβ in Alzheimer's Disease, increased cognitive deficits[1] and reduced synaptogenesis[2]. The usage of PKCε activators such as DCP-LA and Bryotstatin-1 have been shown to reverse such effects[3,4]. PKCε has also been proposed as an oncogene and emerging tumor marker, which leads to the development and clinical trials for PKCε inhibitors[5].

Much effort has been made to characterize the role of PKCε in cellular signaling. However, many challenges remain due to the highly complex nature of PKCε signaling. Firstly, PKCε is involved in compartmentalized cellular signaling that triggers site-specific behavioral phenotypes[6–8]. For instance, addition of phorbol ester 4β-phorbol-12-myristate-13-acetate (PMA) results in accumulation of PKCε at the plasma and nuclear membranes[9]. PKCε has also been reported to localize in Golgi apparatus[10] and mitochondria[11], modulating the functions of each organelle respectively. Secondly, PKCε is activated for varied periods of time in different circumstances[12,13]. The PKCs could undergo acute activation in the presence of GPCR or tyrosine kinase agonists, and a more sustained activation window is observed when agonists such as PMA are added[14]. Genetic overexpression and silencing experiments could also be affected by compensation effects. Most studies utilize chemicals, such as phorbol ester activators and inhibitors, for acute control of PKCε activity. However, these methods result in global changes in PKCε activity, and do not allow for compartmentalized dissection of PKCε signaling. In addition, off-target effects such as the simultaneous activation of other kinases and different PKC isoforms make it difficult to unravel PKCε signalling. Furthermore, since many of these inhibitors or activators cannot be metabolized, sustained modulation of PKCε occurs and results in poor temporal control[14]. Thus, obtaining a full grasp of PKCε signaling activities would require a more specific and precise method for dissection of specific pathways.

To overcome these hurdles, optogenetic systems are often used that allow for the precise spatiotemporal control of protein activation. The optogenetic systems have been used successfully to control the activity of kinases such as AKT1[15,16], cRAF[17], and TrkA[18]. In the present

study, we have adopted optogenetics as a highly suitable approach for dissecting PKCε signaling cascades without the interference of other signaling nodes.

Results

Ideal Characteristics of Opto-PKCε

Engineering optical control of kinases requires the following considerations. Firstly, activation of opto-kinases should be controlled only by light without the need of exogenous factors. This will confer minimal dark background activation and full activation upon light illumination. Secondly, the downstream targets of the opto-kinase should resemble the kinase that it models. Thirdly, activation of the opto-kinase should be reversible and can be configured to activate at specific subcellular sites. In our study, we constructed an optically controllable PKCε that overcomes the limitations of current methods so as to precisely dissect PKCε signaling (**Figure 1A**).

Rational engineering of Opto-PKCε

PKCε activation involves the binding of membrane-resident diacylglycerol, which induces conformational changes and the release of the autoinhibitory pseudosubstrate site, resulting in the phosphorylation of three key signaling sites, Thr566, Thr710 and Ser729. (**Figure 1B**) Thr566 is phosphorylated by pyruvate dehydrogenase kinase 1 (PDK1) in a phosphoinositide-dependent manner, which leads to the autophosphorylation of two residues, Thr710 and Ser729 at the C-terminus[19]. Given that the first phosphorylation event initiated by PDK1 is canonically associated with the activation state of PKCε, it is critical to take into consideration the dependency of the phosphorylation sites for optimal optical control when designing the Opto-PKCε tool.

Considering that PKC stimulation results in self-association through intramolecular and intermolecular interactions between the regulatory and catalytic domains[20–22], we tested if PKCε activation by PMA results in oligomerization of PKCε. We observed that mCherry-PKCε oligomerized after 5 minutes of PMA treatment (Figure S1). This result suggests light-induced oligomerization could be used to promote PKCε activation.

The endogenous PKCε consists of the regulatory domain (C2 and C1 domains) and the catalytic domain (C3, C4 domains and the AGC terminal). Referring to previous work on the phosphoinositide kinases[23], Opto-Raf[24] and Opto-AKT[25], removal of the regulatory domain is typically needed to achieve full optical control of the optogenetic system. In place of the original regulatory domain, the mCherry-cryptochrome 2 (CRY2) construct was fused to the catalytic domain (**Figure 1B**). The CRY2 system has previously been known to promote oligomerization under blue light illumination.

Seven different constructs were tested in the optimization process and subjected to either dark or 15 minutes of blue light. Background PKCε activity was observed when the full catalytic domain was present while activity was reduced when Thr566, Thr710 and Ser729 were mutated to alanine. The difference in PKCε activity under dark and light conditions was further enhanced when the AGC terminal was removed. As such, we termed the fusion protein containing mCherry-CRY2 coupled with PKCε catalytic domain Ala566 and a truncated AGC terminal as Opto-PKCε (**Figure 1C**).

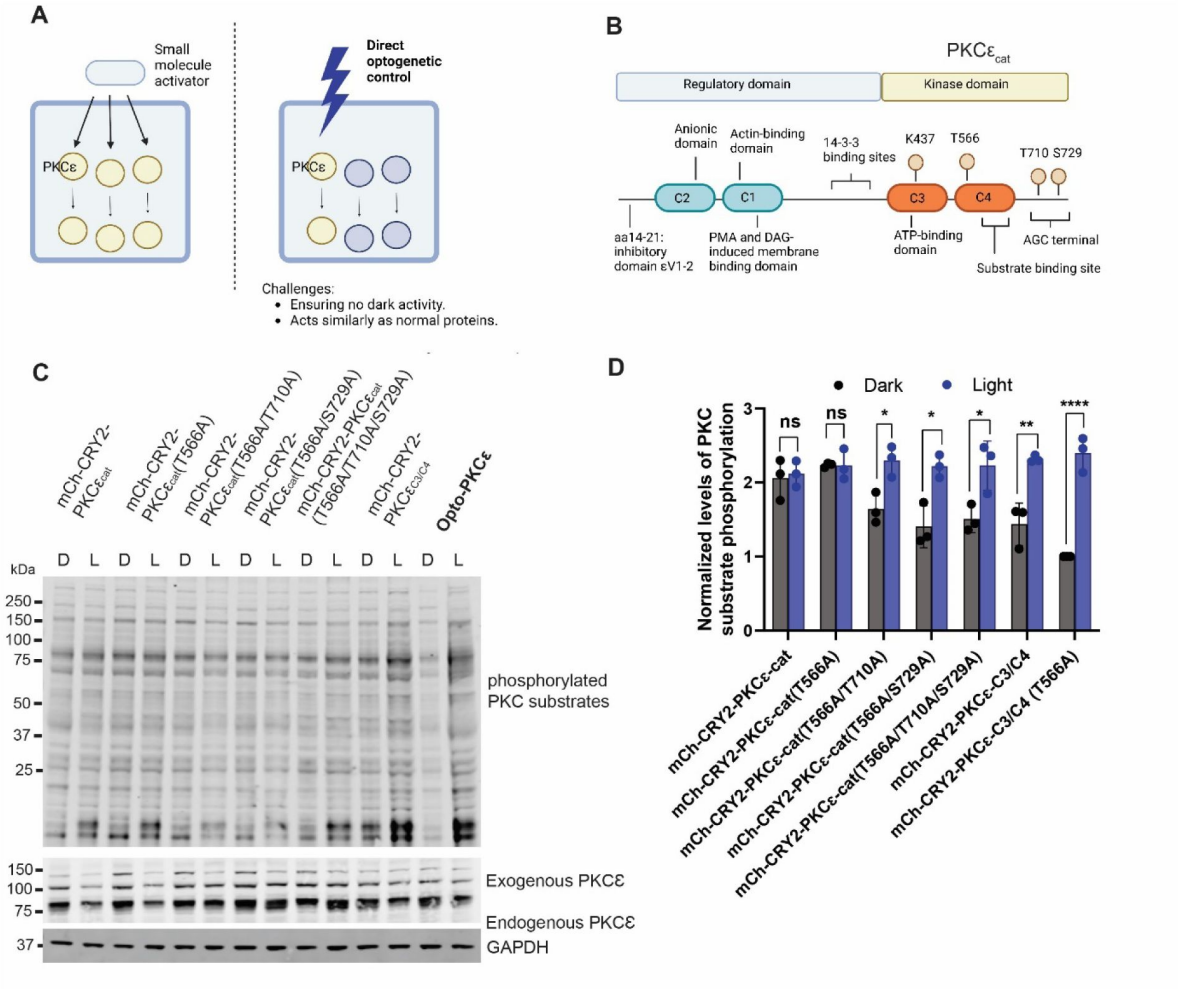

Figure 1

Design and development of Opto-PKCε

(a) Schematic of the ideal properties of an optically-controlled PKCε. Small molecule activators possess off-target effects, without spatiotemporal specificity. Direct optogenetic control of PKCε could allow dissection of the pathway if the challenges listed could be overcome.
(b) Schematic of the regulatory and catalytic domains of PKCε. The regulatory domain of PKCε was truncated and replaced by the blue light sensitive cryptochrome domains tagged with mCherry fluorescent protein.
(c) Representative Western blots of phosphorylation levels of PKCε substrates, PKCε and GAPDH for HEK293T cells transfected with constructs listed. These cells were either subjected to 5 minutes of dark condition or blue light.
(d) Quantification (n=3) of normalized phosphorylation levels of PKCε substrates relative to GAPDH. The data is presented as mean +/− SD.

Molecular dynamics simulations to understand the mechanisms of Opto-PKCε

To understand why the T566A mutation caused reduced kinase activity in the dark for Opto-PKCε, molecular dynamics (MD) simulations were performed to understand the conformational differences between T566-phosphorylated PKCε and the T566A mutant PKCε without the AGC terminal. As there were no available experimental structures of the catalytic domain of human PKCε, we used the AlphaFold model of human PKCε as the initial structure for the simulations[26]. This structure had the activation loop in an active conformation, where Thr566 was in close proximity with the positively charged residues Arg531 and Lys555. Conventional molecular dynamics (cMD) simulations were performed on the kinase domain of PKCε phosphorylated at Thr566 and the T566A mutant without the AGC terminal. Hydrogen bond occupancy analysis revealed that the negatively charged phosphate side chain of phosphorylated Thr566 (pThr566) forms intimate salt bridges with the positively charged side chains of Arg531 and Lys555, with average occupancies of more than 90% (97.9 ± 3.4 % and 90.1 ± 0.5 % respectively). These salt bridges stabilised the activation loop in the active conformation. When Thr566 was mutated to Ala, it did not interact with Arg531 and Lys555, which suggests that the active conformation of the activation loop could be unstable. The mutant PKCε showed slightly higher Cα root mean square fluctuations (RMSF) in a small region of the activation loop (residues 566–573) compared to phosphorylated PKCε (Figure S2A).

To determine if the activation loop underwent further conformational changes as a result of Thr566 phosphorylation and T566A mutation, we performed accelerated molecular dynamics (aMD) simulations to enhance conformational sampling. In these simulations, a boost potential was applied to lower the energy barriers for conformational transitions so that they could occur within a shorter timescale. The aMD simulations showed that the activation loop adopted significantly different conformations in the two systems (**Figure 2A**, Figure S2B and C). Compared to the cMD simulations, the dynamics of the phosphorylated PKCε was very similar, with the activation loop remaining in the active conformation and pThr566 in contact with Arg531 and Lys555, while the activation loop in mutant PKCε shifted towards the ATP binding site. In one aMD simulation run of mutant PKCε, this shifting of the activation loop was accompanied by an outward displacement of the αC helix (**Figure 2A**). This was likely to be an intermediate state between the active and inactive conformations of the activation loop. In the inactive conformation, the activation loop blocked the substrate from binding near the ATP binding site, thus preventing phosphorylation from occurring. These findings suggest that phosphorylation at Thr566 helps to stabilise the active conformation of the activation loop in PKCε and that the T566A mutant PKCε construct we used to form our Opto-PKCε tends towards the inactive conformation, thus accounting for the mutant construct's reduced catalytic activity in the dark.

To determine the requirements for Opto-PKCε to be effectively light-gated, we examined the nature of the residues on the three key signaling sites. First, we compared Opto-PKCε with the construct containing phosphomimetic mutations (sites mutated to negatively-charged residues). We also compared constructs where Thr566 was mutated to glycine or valine, which are similar to alanine mutation. Opto-PKCε dead, which contains a K437R mutation that abrogates the ability to bind to ATP, was included as the negative control (Figure S3A). While the glycine and valine mutants showed similar light-dark properties as the Opto-PKCε, the triple negatively-charged mutant demonstrated higher levels of PKCε activity even in the dark state. This result implies that the charged activation at the signaling sites are crucial for mediating the catalytic domain's activities, and the AGC terminal also affects PKCε activity control (Figure S3B).

Next, we examined how the positioning of the PKCε domain in the construct affects PKCε activation. We examined four constructs containing the optimized PKCε catalytic domain, namely mCherry-CRY2-PKCε (Opto-PKCε), CRY2-mCherry-PKCε, PKCε-CRY2-mCherry and PKCε-mCherry-

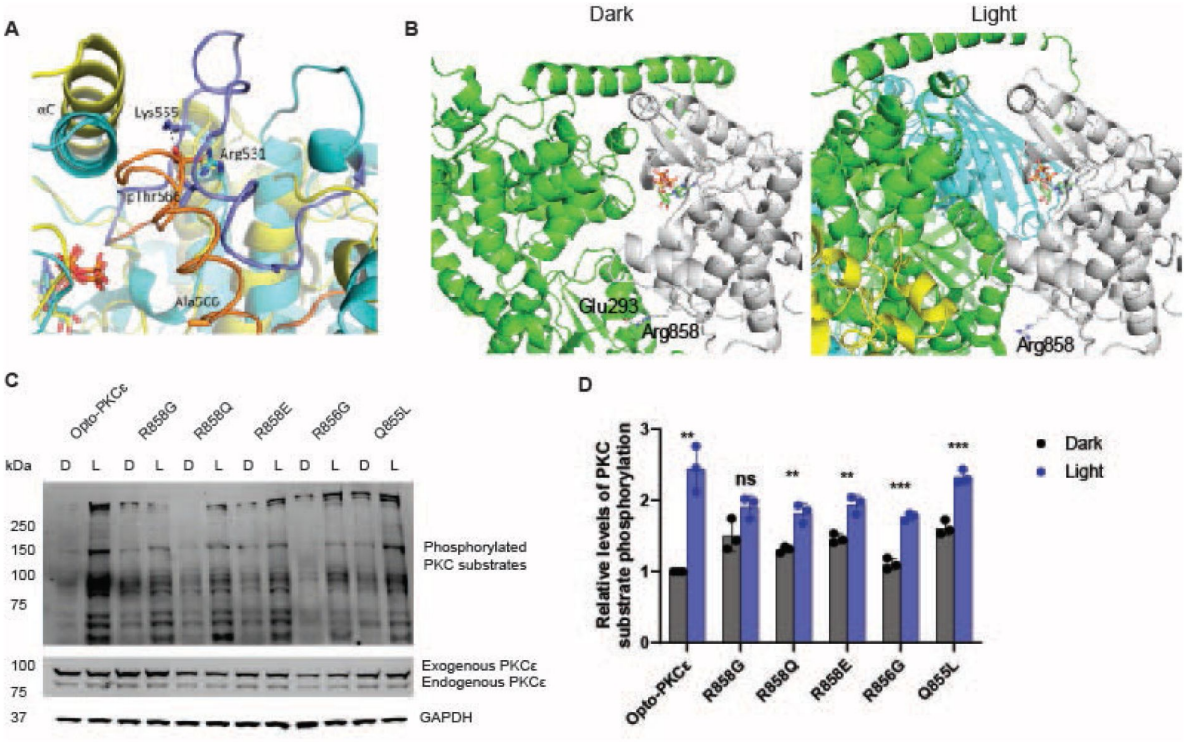

Figure 2

Computational simulations to aid in rationalization of Opto-PKCε dark-light activity.

(a) Superposition of the final trajectory structures from representative aMD simulations of phosphorylated (cyan) and T566A mutant (yellow) PKCε. The activation loops of phosphorylated and T566A mutant PKCε were shown in purple and orange cartoon, respectively.
(b) AlphaFold3 models of the monomeric (left) and tetrameric (right) Opto-PKCε reveal the Glu293-Arg858 interaction as a potential gatekeeper for dark-light activity. The PKCε domain is shown in white while the rest of the protein is shown in green. Other monomers in the tetramer are shown in yellow and cyan. Glu293, Arg858 and ATP are shown in sticks.
(c) Representative Western blots of phosphorylation levels of PKCε substrates, PKCε and GAPDH for HEK293T cells transfected with constructs listed. These cells were either subjected to 5 minutes of dark condition or blue light.
(d) Quantification (n=3) of normalized phosphorylation levels of PKCε substrates relative to GAPDH. The data is presented as mean +/− SD.

CRY2. These constructs were subject to 15 minutes of darkness or blue light. Western blot analysis revealed that the activation of PKCε occurred only when the PKCε domain was fused at the C-terminus (Figure S3C).

Structural modeling with AlphaFold3 to understand interactions gating dark-light activity of Opto-PKCε

We also seek to rationalize the gating of dark-light activity of Opto-PKCε. To this end, we used AlphaFold3 to predict structures of the CRY2 tetramer in light and its monomeric form in dark. The respective top-ranked models of the monomer and tetramer generated by AlphaFold3 suggest that tetramerization led to increased accessibility of the substrate binding site and ATP binding pocket, thus increasing kinase activity. In the monomer, the CRY2 and PKCε domains are in close contact, thus hindering substrate binding and restricting access to the ATP binding pocket. One of these interdomain interactions is the Glu293-Arg858 salt bridge, which is lost upon tetramerization. Nearby residues Arg856 and Gln855 may also be implicated. (**Figure 2B**) The loss of these interdomain interactions in the tetramer leads to the partial release of the PKCε domain from the CRY2 domain, thus increasing accessibility of the substrate and ATP binding sites, and consequently enzyme activity. To validate our hypothesis, we carried out mutations on Arg858, Arg856 or Gln855 and subjected these constructs to dark / light treatment. (**Figure 2C**) Mutation of Arg858 to glycine, glutamine (neutral) or glutamate (negative) consistently results in lower dynamic range of the dark-light activity, where PKC substrate phosphorylation level is higher in the dark and lower under blue light. (**Figure 2D**) This highlights the potential importance of residue Arg858 as a gatekeeper for the optical control of kinase activity. Mutation of Arg856 to glycine did not affect the PKC activity at dark, but results in lower PKC substrate phosphorylation level under blue light. All in all, the mutation analysis confirms the AlphaFold predictions where Arg858 and nearby residues play a key role in gating Opto-PKCε activity, where interactions such as Glu293-Arg858 may stabilize a conformation of Opto-PKCε that reduces accessibility of the ATP binding pocket to the substrate in the dark, and the absence of such interactions in light enables Opto-PKCε to phosphorylate substrates.

Reversibility of Opto-PKCε

An advantage of intracellular optogenetic tools is the temporal control of the system. We subjected the cells transfected with Opto-PKCε to 15 minutes of blue light before 4 hours of darkness. The cells were then reactivated with 10 minutes of blue light. Western blot analysis revealed that the phosphorylation level of PKCε substrates remained high for the first 30 minutes before the substrates were dephosphorylated. Reactivation of the Opto-PKCε construct was achieved, thereby showcasing the reversibility of the system (Figure S4).

Immuno-enrichment of Flag-Opto-PKCε and Flag-PKCε reveals similar substrate interactions

To confirm that Opto-PKCε functions similarly as endogenous PKCε, we next asked if the interactome of Opto-PKCε and PKCε are overlapping. We subjected HEK293T cells transfected with FLAG-tagged Opto-PKCε to five minutes of blue light and performed co-immunoprecipitation experiments to capture the proteins bound to the agarose FLAG beads (**Figure 3A**). Comparing the lists of proteins associated with FLAG-Opto-PKCε and FLAG-PKCε, we found that 238 out of 254 proteins are associated with both, while only 9 proteins each exclusively associate with each subset (**Figure 3B**, Table S1). The list of overlapping substrates includes PKCε, 14-3-3 proteins and MARCKS, which have been well validated in the past to be PKCε-associated proteins. These results reveal that the nature of the Opto-PKCε interactome to be similar to that of PKCε.

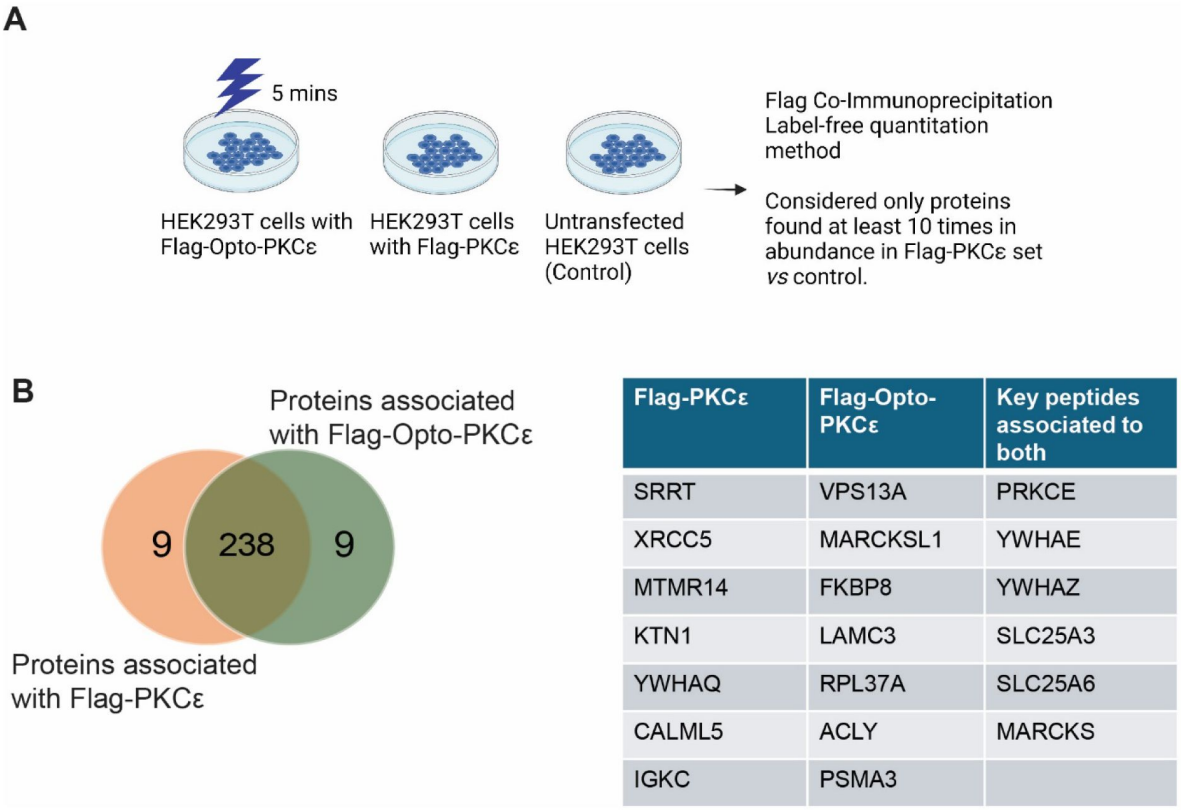

Flag-PKCε	Flag-Opto-PKCε	Key peptides associated to both
SRRT	VPS13A	PRKCE
XRCC5	MARCKSL1	YWHAE
MTMR14	FKBP8	YWHAZ
KTN1	LAMC3	SLC25A3
YWHAQ	RPL37A	SLC25A6
CALML5	ACLY	MARCKS
IGKC	PSMA3	

Figure 3

Opto-PKCε maintains largely similar interactome as that of PKCε.

(a) Schematic of the workflow comparing interactome of Flag-Opto-PKCε and Flag-PKCε. Untransfected HEK293T cells was used as a negative control, with proteins found at least 10 times more in abundance considered for analysis.
(b) Mass spectroscopy of proteins associated with Flag-Opto-PKCε or Flag-PKCε demonstrates that Flag-Opto-PKCε has a largely similar interactome as Flag-PKCε. Key proteins belonging to exclusively each subset or overlapping set is detailed.

Comparison of signaling pathways activated by Opto-PKCε and PMA induction

Although previous studies have profiled cellular responses to PKCε activation by phorbol esters, the activators are also known to activate multiple pathways including PKA and other members of the PKC family. In contrast, Opto-PKCε allowed us to understand the direct downstream targets of PKCε exclusively (**Figure 4A**). To investigate the signaling pathways activated by Opto-PKCε and PMA, we subjected HEK293T cells to the following conditions. HEK293T cells expressing Opto-PKCε were stimulated with blue light for 15 minutes. In a separate set, HEK293T cells were exposed to PMA for 15 minutes.

We first performed Western blot analysis on these cells to track their signaling patterns at 0, 5, 10 and 15 minutes of blue light exposure. As expected, both stimulation approaches resulted in an increase in phosphorylation levels of PKC substrates. However, only PMA caused PKA substrate phosphorylation (**Figure 4B**).

To broadly search for the downstream modules that could be activated by Opto-PKCε and PMA, we performed phosphoproteomics to have a comprehensive phosphorylation map. The lysates were collected and analyzed after stimulation. A comparison of the two conditions was detailed in Table S2. Out of 2196 phosphopeptides detected by phosphoproteomics, 159 phosphopeptides were found to be exclusively phosphorylated in the PMA treatment group, while 156 phosphopeptides were only observed in the Opto-PKCε activation group (**Figure 4C**). Ser163/Ser167 of MARCKS, well documented phosphorylation sites by PKCε, were indeed found to be phosphorylated under both conditions[27]. Notably, PKCδ and MAPK1 were activated only by PMA and not Opto-PKCε, thereby suggesting that these substrates could be off-target effects attributed by PMA.

We then compared the peptides that had significant differences in phosphorylation levels in both conditions, as normalized to total protein levels (Data S1). Some of the more significant proteins were highlighted in the volcano plot in Figure S5A. 80 and 143 peptides were found to be more phosphorylated in Opto-PKCε and PMA conditions respectively for phosphopeptide quantification. We then conducted Kinase-Substrate Enrichment Analysis (KSEA) to estimate overall changes in a kinase's activity based on the collective phosphorylation changes of its identified substrates[28]. We found that CSNK and GSK3 substrates were enriched in the Opto-PKCε activation group while PKA and other PKC pathways were enriched in the PMA treatment group (**Figure 4D**). We further validated this observation with Kinase Enrichment Assay (KEA), which allowed us to examine whether the gene sets from these two conditions were enriched with genes known to interact with kinases[29]. The results further confirmed the activation of pathways independent of PKCε-mediated pathways, such as PKA in the PMA-enriched subgroup (**Figure 4E**). Subsequently, we validated the increase in GSK3B and p38 phosphorylation in the Opto-PKCε subgroups (Figure S5B and C). On the other hand, the activation of MAPK1 was seen exclusively in the PMA subgroup (Figure S5C).

Opto-PKCε can be customized to be activated at specific subcellular locations

While Opto-PKCε activation was seen in the entire cell, which was evident from the phosphorylation of proteins in all major subcellular compartments (Table S3), physiological activation of PKCε was usually site-specific. For instance, the translocation of PKCε to the plasma membrane has long been regarded as a readout for PKCε activation. In separate studies, PKCε has also been shown to be activated at the mitochondria, where PKCε phosphorylates the

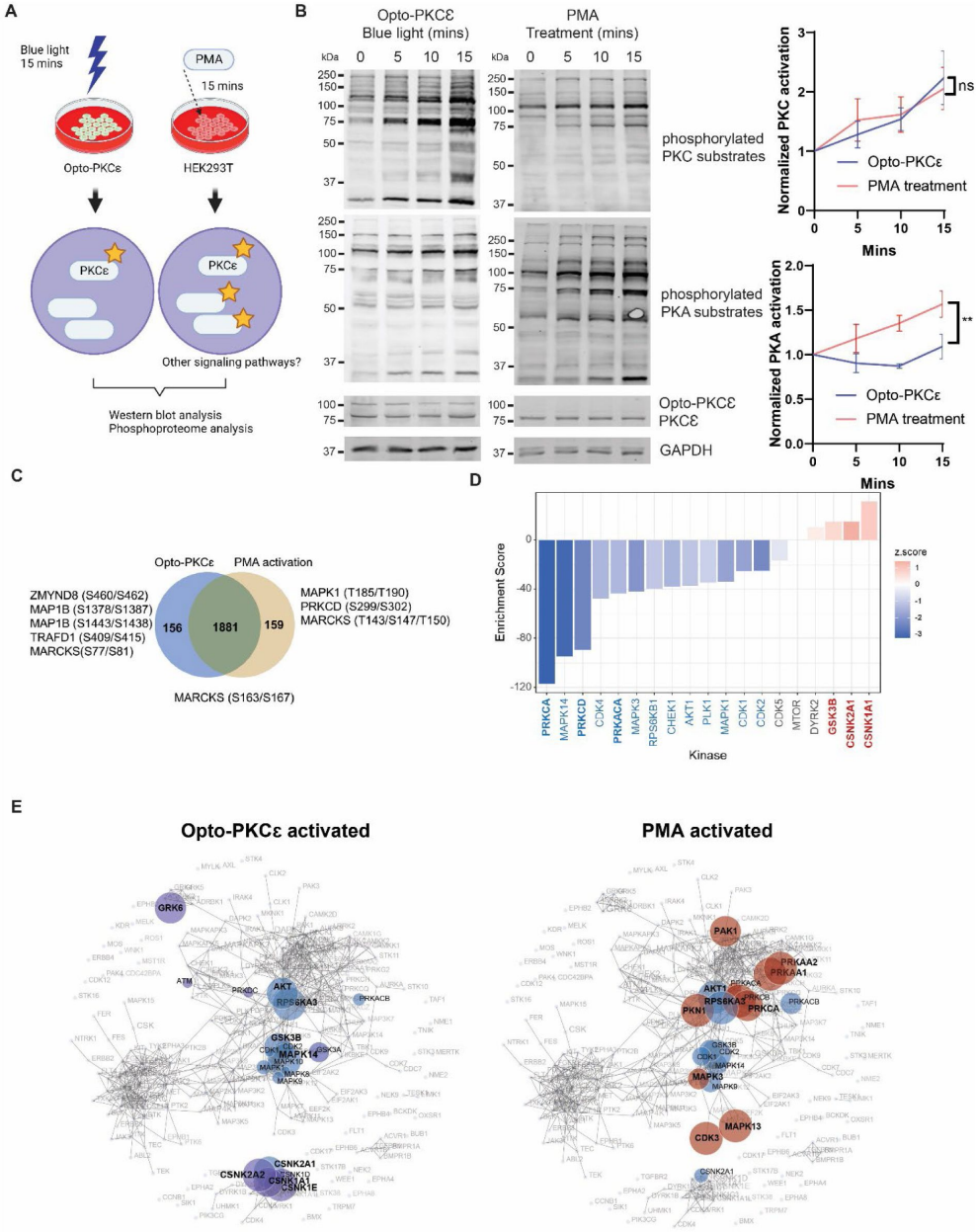

Figure 4

Opto-PKCε enables dissection of PKCε signaling.

(a) Schematic of the experiments comparing signaling dynamics arising from 15 minutes of Opto-PKCε activation and PMA induction respectively.
(b) Representative Western blots of phosphorylation levels of PKC and PKA substrates, PKCε and GAPDH for HEK293T cells subjected to both conditions. Quantification (n=3) of normalized phosphorylation levels of PKC and PKA substrates relative to GAPDH.
(c) Venn Diagram of phosphopeptides quantifying the number of phosphopeptides appearing in both subsets or in either subset. Some of the main phosphopeptides known to be activated by PMA or classical PKCε phosphosites are highlighted.
(d) KSEA revealed that CSNK and GSK3 substrates were enriched in opto-PKCε activation group while PKA pathways and other PKC pathways were enriched under PMA treatment.
(e) KEA validated the increased phosphorylation of CSNK and GSK3 substrates under opto-PKCε activation (in purple) and those of PKA substrates (in red) under PMA treatment. Common substrates are highlighted in blue.
The data in **(b)** are presented as mean +/− SD.

mitochondrial KATP channel in order to protect against ischemic insults[30,31]. To understand the activity of PKCε at specific subcellular locations, it is necessary to manipulate the selective recruitment of Opto-PKCε to the desired sites.

CRY2 forms heterodimers with crytochrome-interacting basic-helix-loop-helix 1 protein (CIB1) upon blue light stimulation. We made use of this feature to pair Opto-PKCε with fusion proteins of the N-terminus truncated version of CIB1 (aa 1-170), CIBN, tagged to cellular location markers[32]. Specifically, CIBN-GFP-miro and CIBN-GFP-CAAX were localized at the outer membrane of the mitochondria and plasma membrane respectively, allowing PKCε activation at these locations upon blue light recruitment (**Figure 5A**). Upon blue light stimulation, Opto-PKCε translocated to the plasma membrane in HEK293T cells co-transfected with Opto-PKCε and CIBN-GFP-CAAX (**Figure 5B**). Similarly, Opto-PKCε translocated to the mitochondria in HEK293T cells co-transfected with Opto-PKCε and CIBN-GFP-miro1 under blue light excitation (**Figure 5B**).

Using subcellular fractionation, we tested whether the recruitment of oligomerized Opto-PKCε to the different subcellular locations causes the local phosphorylation of PKC substrates. Indeed, when the HEK293T cells co-transfected with Opto-PKCε and CIBN-GFP-CAAX were exposed to blue light, phosphorylation of PKC substrates selectively increased only at the plasma membrane. When the localization tag was replaced with CIBN-GFP-miro, the increase in phosphorylation of PKC substrates occurred exclusively in the mitochondrial fraction (**Figure 5C**). Next, we tested whether the recruitment of Opto-PKCε from the cytosol is a necessary event, or if the same effect can be achieved if Opto-PKCε was already tagged to the desired localization. Interestingly, in the event where Opto-PKCε was constitutively localized at the plasma membrane through myristylation tag, the increase in phosphorylation of PKC substrates at the plasma membrane was less prominent (**Figure 5D**).

Sustained PKCε activation at the plasma membrane of hepatocytes results in phosphorylation of the insulin receptor at Thr-1160

The role of hepatic PKCε in lipid-induced hepatic insulin resistance, particularly whether PKCε alone is responsible for phosphorylation of insulin receptor at Thr1160 in hepatocytes [33,34,35], has been under debate. Opto-PKCε tool is perfectly positioned to answer the question – (1) the use of the tool occurs in intact cells where only PKCε, and not other kinases, is selectively and precisely activated at the plasma membrane; (2) the duration of the activation can be tuned to investigate the nature of the interaction; (3) in contrast, drugs and genetic manipulation may cause compensatory effects, which may result in an indirect effect towards PKCε activation. We first checked the utility of the Opto-PKCε tool in isolated mouse hepatocytes and compared its activation in the cytosol versus the plasma membrane. Hepatocytes co-transfected with CIBN-GFP-CAAX and Opto-PKCε showed an increase in PKC substrate phosphorylation specifically at the plasma membrane (**Figure 6A**). Upon confirmation of the utility of Opto-PKCε tool in hepatocytes, we investigated whether PKCε activation alone at the plasma membrane would result in phosphorylation of insulin receptor at Thr-1160. Hepatocytes co-transfected with CIBN-GFP-CAAX and Opto-PKCε showed an increase in phosphorylation of insulin receptor at Thr1160 under blue light stimulation while this was not observed in hepatocytes transfected with only Opto-PKCε, highlighting the need for PKCε to be localized at the plasma membrane for the insulin receptor Thr1160 phosphorylation (**Figure 6B**). At the same time, this translated to a significant decrease in insulin-stimulated IRK Thr-1158/1162/1163 phosphorylation level for plasma membrane activation of PKCε. As a negative control, hepatocytes co-transfected with CIBN-GFP-CAAX and Opto-PKCε (dead) did not show any increase in phosphorylation of the insulin receptor at Thr-1160. In the absence of insulin, we noted an increase of the insulin receptor Thr1160 phosphorylation level as well (Figure S6). Lastly, we examined whether the Opto-PKCε needed to be constitutively localized at the plasma membrane for the insulin receptor Thr1160 phosphorylation. A transient bout of 15 minute Opto-PKCε

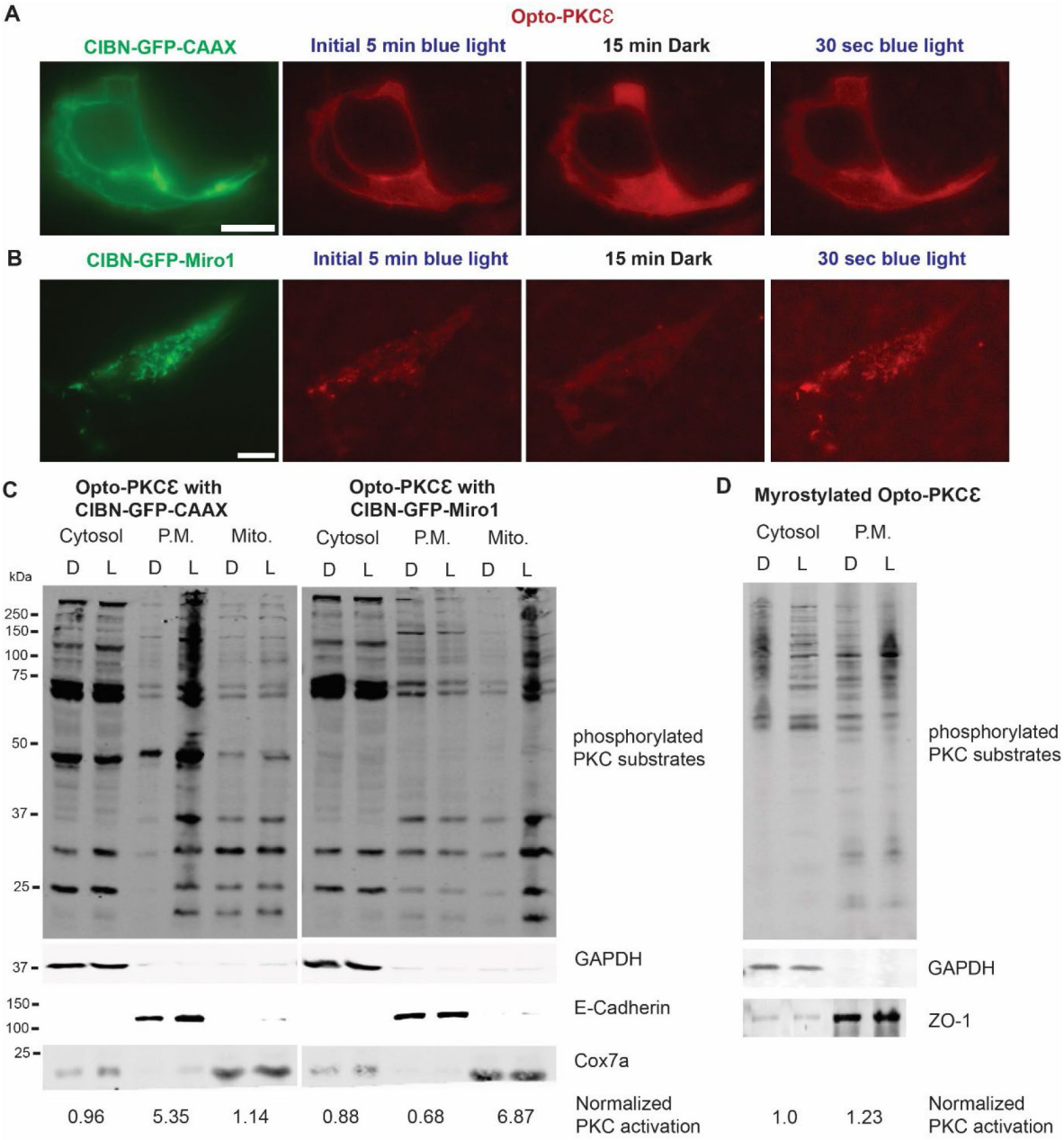

Figure 5

Opto-PKCε enables subcellular dissection of PKCε signaling.

(a) Representative images of HEK293T cells transfected with Opto-PKCε and CIBN-GFP-CAAX from initial 5 min blue light to 15 minutes dark and then back to blue light exposure. CIBN-GFP-CAAX could be found to colocalize with Opto-PKCε after 30 seconds of blue light exposure. Scale bar = 10 μm
(b) Representative images of HEK293T cells transfected with Opto-PKCε and CIBN-GFP-miro1 from initial 5 min blue light to 15 minutes dark and then back to blue light exposure. CIBN-GFP-miro1 could be found to colocalize with Opto-PKCε after 30 seconds of blue light exposure. Scale bar = 10 μm
(c) Western blot analysis of subcellular fractionation experiment depicting phosphorylation of PKC substrates, E-cadherin, Cox7a and GAPDH of cells containing Opto-PKCε with CIBN-GFP-miro1 or CIBN-GFP-CAAX and subjected to 15 minutes of dark or blue light.
(d) Western blot analysis of subcellular fractionation experiment depicting phosphorylation of PKC substrates, ZO-1 and GAPDH of cells containing myr-Opto-PKCε and subjected to 15 minutes of dark or blue light.

activation at the plasma membrane was not sufficient to sustain the insulin receptor phosphorylation at Thr1160, indicating the temporal dependence of PKCε at the plasma membrane for the insulin receptor phosphorylation. (**Figure 6C**)

PKCε activation at the mitochondria results in reduced oxygen consumption rate

To investigate the role of PKCε activation at the mitochondria, we employed the Opto-PKCε tool coupled with CIBN-GFP-miro which was tagged at the outer mitochondrial membrane. We performed mitochondrial stress assays and measured the oxygen consumption rate (OCR) using different inhibitors to probe the bioenergetics parameters. **Figure 7A** showed the OCR of transfected HEK293T cells with or without blue light. Basal and ATP-dependent OCR readings indicate that PKCε activation at the mitochondria induced by light resulted in a lower OCR. We quantified the basal, ATP production, proton leak and spare capacities and found that light treatment significantly reduced these four parameters (**Figure 7B**). To ensure that this was not triggered by off-target effects due to blue light, we performed the mitochondrial stress assays on CIBN-GFP-miro-transfected cells with or without blue light, and did not observe any significant difference in the bioenergetics (**Figure 7C**).

To identify potential candidates associated with the bioenergetics phenotype, we listed the top phosphorylated mitochondrial substrates by PKCε as identified in a kinome-wide assay previously published (**Figure 7D**)[36]. NADH dehydrogenase [ubiquinone] iron-sulfur protein 4, mitochondrial (NDUFS4) was found to be the top candidate, which encodes a nuclear-encoded accessory subunit of the mitochondrial membrane respiratory chain NADH dehydrogenase (complex I). Indeed, phosphorylation of NDUFS4 was observed when PKCε activation at the mitochondria was induced by blue light (**Figure 7E**). This could explain the reduction in Complex I activity upon PKCε activation at the mitochondria[6].

Discussion

With more than 60,000 PubMed entries, PKC is one of the most well-studied kinases, and its many isozymes have been extensively characterized. However, it has been challenging to distinguish and disentangle the intricate signaling network of each PKC isozyme, and how the distinctive patterns caused by the activation of each PKC isozyme could lead to a vast range of cellular responses[37]. Due to the inherent limitations of traditional genetic tools and small molecule potentiators of PKC activity, the complexities of PKC activity and function have yet to be resolved.

Optogenetic control of individual PKC isozyme activity is an attractive strategy to address these fundamental questions. A typical approach in the field is to mimic the localization patterns of the intracellular proteins in its activation. This technique has been successfully utilized for the activation of PI3K[23], Ras/Raf/ERK[24,38], Bax[39] and Rho-GTPases[40,41]. Indeed, a similar approach has been utilized by Logothetis and colleagues to recruit the catalytic domain of PKCε to the plasma membrane[42]; the activation of GIRK1/4 was the readout for PKCε activation. However, it is important to note that PKCε has been shown to exert signaling effects on multiple subcellular locations, such as Golgi[10], mitochondria[30,31] and nucleus[43]. As such, it is important to ensure the background activity of opto-PKCε is effectively eliminated, and that the presence of blue light would be the only trigger required to activate the ideal opto-PKCε construct. This is the first report of an PKCε optogenetic tool with reduced background activation that may potentially affect the cellular signaling dynamics.

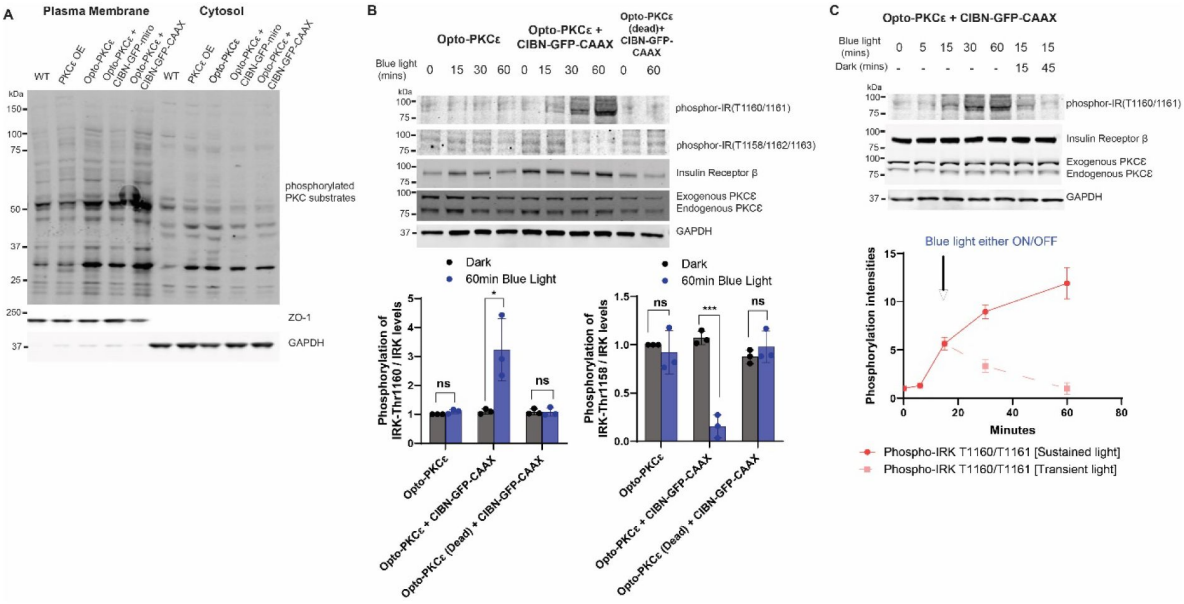

Figure 6

Sustained PKCε activation at the plasma membrane of hepatocytes results in phosphorylation of Insulin Receptor at Thr-1160.

(a) Western blot analysis of subcellular fractionation experiment depicting phosphorylation of PKC substrates, ZO-1 and GAPDH of primary hepatocytes containing transfected plasmids as listed and subjected to 15 minutes of dark or blue light.
(b) Representative Western blots of phosphorylation levels of phosphor-IRK (T1160/T1161), phosphor-IRK (T1158/T1162/T1163), Insulin Receptor, PKCε and GAPDH for primary hepatocytes subjected to stated conditions. Quantification (n=3) of normalized phosphorylation levels relative to insulin receptor levels.
(c) Representative Western blots and phosphorylation levels of phosphor-IRK (T1160/T1161), Insulin Receptor, PKCε and GAPDH for primary hepatocytes subjected to stated conditions. Quantification (n=3) of phosphor-IRK (T1160/T1161) relative to Insulin Receptor levels.
The data in **(b)** and **(c)** are presented as mean +/− SD.

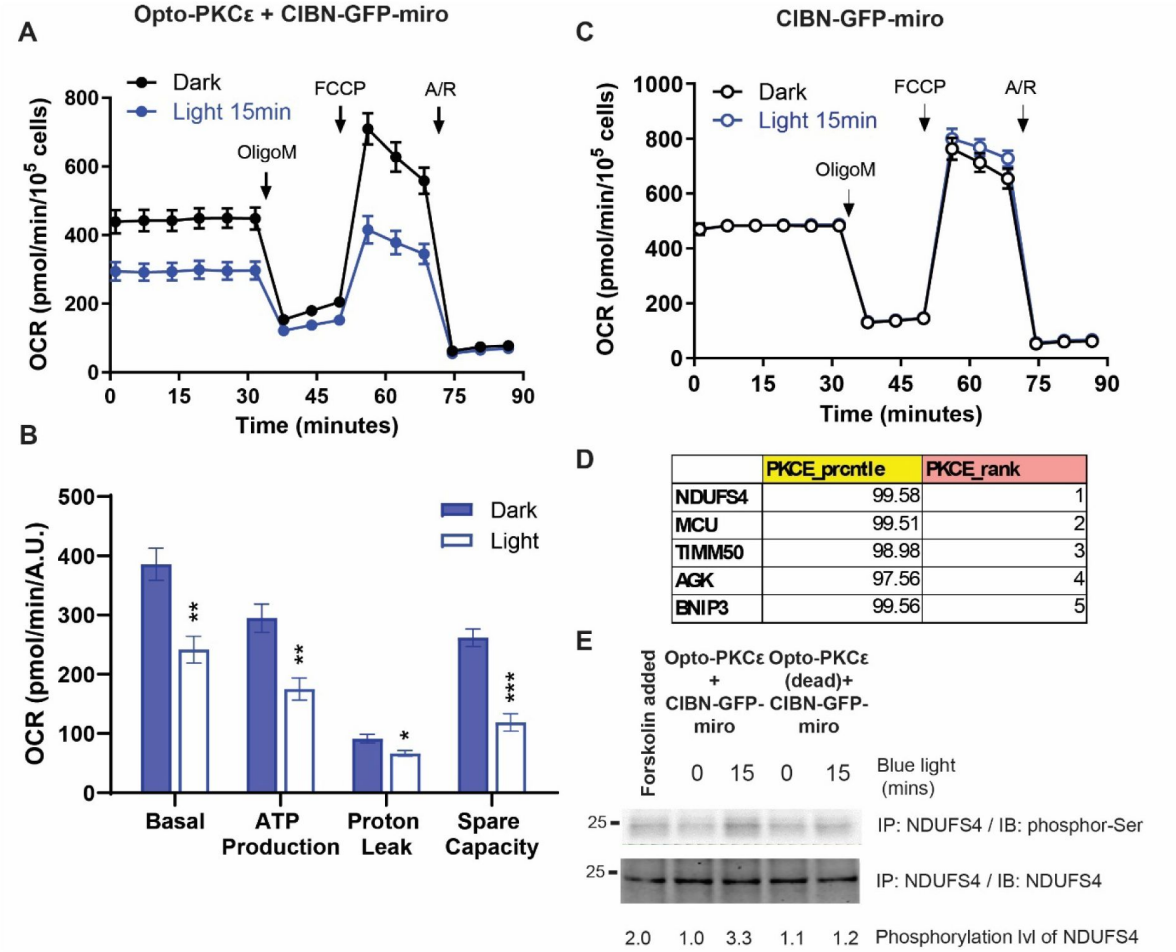

Figure 7

PKCε activation at the mitochondria results in reduced oxygen consumption rate.

(a) HEK293T cells transfected with Opto-PKCε and CIBN-GFP-miro were subjected to 15 minutes of either dark or blue light. Oxygen Consumption Rate (OCR) measurements were then obtained with an extracellular flux analyser (Seahorse Bioscience). 4um of Oligomycin, 0.5um of FCCP, 1um of Antimycin A and Rotenone were injected into the cells at different time points preset on the machine and OCR response was recorded. 5 sets of experiments are represented.
(b) Quantification (n=5) of the OCR of HEK293T cells transfected with Opto-PKCε and CIBN-GFP-miro under different conditions.
(c) HEK293T cells transfected with CIBN-GFP-miro were subjected to either dark or 15 minutes of blue light. Oxygen Consumption Rate (OCR) measurements were then obtained with an extracellular flux analyser (Seahorse Bioscience). Similar inhibitor concentrations were used as in (a).
(d) List of top phosphorylated substrates by PKCε that are known to be localized at mitochondria.
(e) Western blots of co-immunoprecipitation experiments of NDUFS4 looking at phosphor-Ser and NDUFS4 levels subjected to stated conditions. Forskolin was added as a positive control.
The data in **(a)** and **(b)** are presented as mean +/− SD.

To achieve minimal background activation of the optogenetic construct, we took reference from previous work on the activation of optoPKA.[44] In that study, mutation of residues at the activation loop allowed the construct to have dark-silent and light-active properties. Hence, we developed an optogenetic strategy that allows us to achieve minimal activity in the dark state. To do so, we inactivated the phosphorylation site Thr566 at the activation loop by mutating the site to an alanine. This is a key requirement to realize the robust light-dark differentiation of Opto-PKCε. We then demonstrated that the removal of the AGC terminal further differentiated the activity of Opto-PKCε under blue light. The AGC terminal is a key regulatory element of protein kinases A, G and C, which help to structure the catalytic core and promote the stability of PKCε through phosphorylation of the turn motif and hydrophobic motif[45]. In our study, we found that the removal of the AGC terminal did not affect the stability of Opto-PKCε but might lessen restriction of the catalytic core, thus allowing activation upon light-induced oligomerization.

We then tested whether Opto-PKCε behaves similarly to endogenous PKCε. Our phospho-proteomics analysis showed that the substrates phosphorylated by Opto-PKCε overlaps greatly with those phosphorylated by endogenous PKC, which affirms that the Opto-PKCε tool does mimic the activity of endogenous PKC. Our phosphoproteomics analysis has also provided further insights into the substrates of PKCε. Notably, MAPK1 was found to be activated only by PMA and not Opto-PKCε. Classical overexpression studies have suggested that Raf, an upstream kinase of MAPK1, and PKCε activate each other[46]. However, a study has demonstrated that PKCε does not activate Raf-1 and could be indirectly stimulating Raf1 by inducing the production of autocrine growth factors[47]. Next, we found that the activation of Opto-PKCε resulted in the activation of p38 pathway, a phenomenon not being observed through PMA induction. Furthermore, previous work has highlighted that the PKCε-p38 axis[48], and its activation could have been potentially masked by other pathways, such as PKA and other PKC isoforms, that are also activated by PMA. Opto-PKCε activation is specific and avoids activating kinase-mediated pathways that can mask signaling pathways regulated by PKCε.

Opto-PKCε also potentially paves the way in understanding phosphosites arising exclusively from PKCε activation, which could be masked by the activation of other signaling pathways. For instance, while MARCKS was activated on the known canonical site (S163/167) by both PMA and Opto-PKCε, S77/S81 phosphorylation was only observed in the Opto-PKCε set while T143/S147/T150 phosphorylation was only observed in the PMA subset. In addition, MAP1B, also known to be phosphorylated by PKCε[49], has additional sites that were phosphorylated by the Opto-PKCε not found in the PMA treatment group. As the functions of the S77/S81 and T143/S147/T150 phosphosites on MARCKS and the phospho-sites on MAP1B are virtually unknown, Opto-PKCε can be a useful tool to unravel the role of these phospho-sites.

In this paper, we have attempted to understand the potential mechanisms driving the dark-light activity of Opto-PKCε. While the oligomerization activity of PKCε upon PMA induction has not been reported before, there have been reports on PKCα oligomerization[20–22]. As such it is not surprising to observe the PKCε oligomerization events due to the higher concentration of PKCε on lipid rafts and potential transphosphorylation activities which would require close proximity[50]. Interestingly, light-induced oligomerization of Raf1 has also shown to induce its activation[17]. Nonetheless, the forced oligomerization of PKCε without the regulatory domain may induce conformational changes in the accessibility of the ATP binding site, which could be a future area of investigation for the design of optogenetic kinases. Alphafold simulations suggest that Glu293-Arg858 intramolecular interactions might play a role in reducing the accessibility of the kinase catalytic domain in the dark state, and the absence of such interaction in the oligomerized light state enables its activity to be reconstituted. The role of Glu293 (Glu42 of cryptochrome) was not included in this study as we hypothesized that the crptochrome oligomerization activity may be affected if mutations were to be performed here. As such, the mutation studies are focused on the residues on PKCε (R502, R500, Q499 corresponding to R858, R856 and Q499 on Opto-PKCε), which

are not located immediately at the ATP binding site. The phosphorylation levels at both dark and light levels were within the original dynamic range of Opto-PKCε activity, suggesting that mutations on these residues did not affect the intrinsic kinase activity.

Unlike previous studies where kinase domains are recruited to plasma membrane to elicit their activity[25,42], the Opto-PKCε tool is not reliant on translocation activity and overcomes the limitations to probe the role of PKCε only on the plasma membrane. Achieving subcellular targeting and probing its downstream signaling are now possible in other subcellular compartments. We also attempted to create a myrostylated form of Opto-PKCε where changes in PKC substrate phosphorylation were not as dramatic when compared to recruitment of Opto-PKCε to the plasma membrane via cotransfection of CIBN-GFP-CAAX and Opto-PKCε. This could be due to the localized high concentration of the myrostylated Opto-PKCε, which may contribute to higher background activity. Further work should focus on fine-tuning the expression levels in attempt to reduce the background activity. In addition, Opto-PKCε sets the stage to study specific phosphorylation events on a PKCε substrate, and such concepts can be extended to other PKC isozymes to understand the signaling dynamics by each individual isozyme.

Previously, PKCε has been shown to be activated by increased plasma membrane associated *sn*-1,2 diacylglycerol levels in hepatic insulin resistance[51]. While we did not observe the landmark event of IRK Thr1160 phosphorylation by both Opto-PKCε and PMA[33,34] in HEK293T cells, we carried out the activation of Opto-PKCε in mouse hepatocytes where we subjected the transfected cells with different spatiotemporal windows of activation. Indeed, the sustained localization of activated Opto-PKCε is required for the IRK Thr1160 phosphorylation, while insulin-stimulated IRK Thr1158/1162/1163 phosphorylation is downregulated. While the Thr1160 phosphorylation event has been convincingly demonstrated in the past in hepatocytes overexpressed with constitutively membrane-localized PKCε and also *in vitro* settings, the experiments performed with the optical PKCε present direct evidence for Thr1160 phosphorylation of IRK by PKCε only if PKCε is localized at the plasma membrane, and if its activation is sustained.

The advent of the tool also allowed us to probe the role of PKCε at other organelles. Traditionally, it has been assumed that PKCε activation is noted by its translocation to the plasma membrane, but some reports have noticed the translocation of PKCε to other locations[6]. For instance, oxidant-induced injury causes PKCε to activate and translocate to the mitochondria in kidney cells and that this activation mediates decreases in mitochondrial function, specifically in complex I-mediated respiration, active Na+ transport, and Na+-K+-ATPase activity[6,52]. Our results support these findings and suggest a potential role of NDUFS4 phosphorylartion by PKCε in mediating the observed phenomena. More studies specifically at finding the site of phosphorylation on NDUFS4 could be carried out for further exploration.

The Opto-PKCε tool could easily be applied to other prevailing questions in biology. For instance, the role of PKCε can be dissected in cancers where different PKC isozymes can have similar, and sometime opposing roles in cell proliferation and other cellular functions[53]. Moreover, the role of PKCε activation in memory formation has yet been elucidated. This could be addressed with the application of Opto-PKCε in rodent brains[54].

Limitations of the study

The Opto-PKCε tool had not been studied for the number of reversible cycles and longer durations to be utilized. More studies could be performed to ascertain the underlying reasons that govern the dark-light activity of Opto-PKCε, for example cryo-EM crystallography could enable the structural features to be studied in detail. Additionally, our optical system requires the use of overexpression systems, so the system may not be easily applicable to cell lines where transfection may be difficult. It is also possible that in our FLAG pulldown experiments that some nonspecific proteins may still be identified despite having negative controls. Lastly, we have not yet applied

the tool to tissues in an animal model; however, we foresee that the deployment of the components using AAVs could ensure targeting to particular tissues without need for additional modifications.

Key resources table

REAGENT or RESOURCE	SOURCE	IDENTIFIER
Antibodies		
PKC epsilon monoclonal anti-Rabbit	Cell Signalling Technology	#2683
Phospho-(Ser) PKC substrate polyclonal anti-Rabbit	Cell Signalling Technology	#2261
Insulin Rb antibody (C-19) polyclonal anti-rabbit	Santa Cruz Biotechnology	sc-57342
Phospho-IRK (T1150/T1151) monoclonal anti-mouse	Sigma Aldrich	04-299
Phospho-IRK (T1163/1162/1158) polyclonal anti-rabbit	Sigma Aldrich	07-841
Phospho-IRK (T1160) monoclonal anti-rabbit	Novo Nordisk	
P44/42 MAPK polyclonal anti-rabbit	Cell Signalling Technology	#9102
Phospho-p44/42 MAPK (Thr202/Tyr204) polyclonal anti-rabbit	Cell Signalling Technology	#9101
P38 MAPK (D13E1) XPI monoclonal anti-rabbit	Cell Signalling Technology	#8690
Phospho-p38 MAPK (Thr180/Tyr182) polyclonal anti rabbit	Cell Signalling Technology	#9211
GSK3b	Cell Signalling Technology	#9315
Phospho-GSK3b (Ser9)	Cell Signalling Technology	#5558S
GAPDH monoclonal anti-mouse	Santa Cruz Biotechnology	sc-32233
NDUFS4 monoclonal anti-mouse	ThermoFisher	MA5-19432
Phospho-Serine	Abcam	Ab9332
E-Cadherin (HECD-1)	ThermoFisher	#13-1700
VDAC	Abcam	ab34726
IRDye® 800CW Goat anti-Rabbit IgG (H + L)	LICOR	926-32211
IRDye® 680RD Donkey anti-Mouse IgG (H + L)	LICOR	926-68070
Alexa Fluor 488 Goat anti-rabbit	ThermoFisher	A11008
4',6-Diamidino-2-Phenylindole, Dihydrochloride (DAPI)	ThermoFisher	D1306
Bacterial and virus strains		
One Shot Stbl3 Comp E Coli	Invitrogen	C737303
Biological samples		
Mouse: C57BL/6	InVivos	N/A
Chemicals, peptides, and recombinant proteins		
Phorbol 12-myristate 13-acetate (PMA)	MedChemExpress	HY-18739
Forskolin PKA Activator	Sigma-Aldrich	F3917
PKCε Inhibitor Epsilon-V1-2 (ε-V1-2)	MedChemExpress	HY-P0154
Fetal bovine serum (FBS)	Gibco	10500064
Horse Serum	Thermofisher Scientific	16050122
Penicillin-Streptomycin (P/S)	Gibco	15140122
Dulbecco's Modified Eagle Medium High Glucose	Cytiva	SH30243.FS
M199 media	Gibco	11150067
Seahorse XF DMEM Media	Agilent	103680-100
Trypsin	Gibco	12605036

Poly-D-Lysine	Gibco	A3890401
ExpiFectamine™ 293 Transfection Kit	Gibco	A14525
Opti-MEM™ I Reduced Serum Medium	Gibco	51985091
PBS, pH 7.4	Gibco	10010023
Collagenase Type TV	Sigma Aldrich	C5138
EGTA	EMD Millipore Corp.	324626
c0mplete, EDTA-free EASYpack	Roche	4693159001
PhosSTOP™ EASYpack	Roche	4906845001
Triton-X100	Sigma Aldrich	9036-19-5
Tween-20	Promega	H5152
4X LDS	Invitrogen	NP0008
Bovine Serum Albumin (BSA)	Capricorn scientific	BSA-1S
10X Tris-Glycine-SDS buffer	BioRad	1610772
10X Tris-Glycine buffer	BioRad	1610771
20X MOPS SDS Running buffer	Invitrogen	NP0001
20X Tris Buffered Saline Buffer	Base Asia	BUF-3030-20X4L
Dimethyl sulfoxide (DMSO)	Sigma Aldrich	D8418
In-Fusion® Snap Assembly Master Mix	Takara USA Bio	638944
FavorPrep Plasmid Extraction Kit	Favorgen Biotech	FAPDE300
PureLink™ HiPure Plasmid Filter Maxiprep Kit	Invitrogen	K210016
Phusion Flash High Fidelity PCR MasterMix	ThermoFisher	F548L
Critical commercial assays		
Minute™ Plasma Membrane Protein Isolation and Cell Fractionation Kit	Invent Biotechnologies	SM-005
Agilent Seahorse XF Cell Mito Stress Test Assay	Agilent	103015-100
Pierce ™ BCA Assay	ThermoFisher	23250
Pierce™ Protein A/G Magnetic Agarose Beads	ThermoFisher	78610
Experimental models: Cell lines		
Human: Human Embryonic Kidney cells HEK293T (female)	ATCC	CRL-3216
Human: HepG2 (Male)	ATCC	HB-8065
Animal: African green monkey kidney fibroblast-like cell-line COS7	ATCC	CRL-1651
Oligonucleotides		
Primers for Opto-PKC tool, see **Table S4**	Present study	N/A
Software and algorithms		
ImageJ	National Institute of Heatlh	N/A
GraphPad Prism	GraphPad Software Inc., La Jolla, CA, USA	N/A
Kinase-Substrate Enrichment App (KSEAapp)	R Studio	N/A
Recombinant DNA		
CIBN-GFP-CAAX	Addgene	#26867
CRY2high-mCherry	Addgene	#104063
Flag-PKCε	Addgene	#10795
Other		
LED light array	ThorLabs	LED465E
XF24 Extracellular Flux Analyzer	Seahorse Biosciences	102238-100

Methods and materials

Cell culture

Human embryonic kidney 293T (HEK293T) and Human hepatoblastoma HepG2 cells were cultured in Dulbecco's Modified Eagle Medium High Glucose (DMEM HG) supplemented with 10% Fetal Bovine Serum (FBS) and 1% Penicillin-streptomycin (P/S).

PC12 cells were cultured in F12-K media supplemented with 15% horse serum and 2.5%FBS. All cell plates were maintained in a standard incubator at 37°C in an atmosphere of 5% CO_2.

Primary mouse hepatocytes

Hepatocytes were isolated from C57BL/6 female mice between 8-12 weeks old. Perfusion buffer containing 1mm EGTA and 5.5mm glucose in HBSS was infused into the liver via the portal vein for 10 mins using a 25G butterfly needle at a speed of 3ml/min. Digestion buffer containing 0.3mg/ml of Collagenase Type TV, 5mm CaCl2 and 5.5mm glucose was thereafter introduced into the liver for 10 mins at a speed of 3ml/min. The liver was subsequently harvested and dissociated with attachment media containing 0.2% Bovine Serum Albumin, 2% Fetal Bovine Serum and 1% Penicillin streptomycin in media M199 media using forceps. Cell suspensions were passed through two 70 µm strainers per liver and underwent centrifugation twice at 50g for 2 mins. The cells were re-suspended and washed in attachment media after each centrifugation. Cell count and viability were performed using trypan blue and an automated cell counter. Tissue culture dishes were pre-coated with 0.1% fish gelatin for 1h and washed twice with PBS (Gibco). Live cells were plated at a density of 10 million per 10cm. Cells were subsequently incubated in a 37°C incubator containing 5% CO2 for 4 hours before attachment was aspirated and replaced with maintenance media containing only M199. Subsequent experiments performed on the isolated hepatocytes were done within 48 hours of isolation.

Proteomics sample preparation (on beads digestion-LC-MS/MS)

Samples were reconstituted with 50 µL of 100mM Triethylammonium bicarbonate (TEAB), followed by adding 50 µL of 2,2,2-Trifluoroethanol (TFE). Samples were then reduced by adding to the final concentration of 10 mM of Tris(2-carboxyethyl) phosphine (TCEP) and incubated at 55°C for 20 minutes shaking at 900 rpm on a thermomixer. The samples were cool down to room temperature before speedvac to remove 2,2,2-Trifluoroethanol (TFE). Around 20 µL of the samples were left and alkylated to final 55mM of 2-Chloroacetamide (CAA) in dark for 30 minutes. All samples were top up to 100 µL with 100mM TEAB and digested with 4 µg of LysC for 4 hours, followed by 4 µg of trypsin overnight at 37°C with thermomixer at 900 rpm.

Desalting was carried out using HLB C18 reversed-phase cartridges. Desalted peptides were reconstituted with 10 µL of 0.1% (v/v) formic acid in water and 2 µL was injected for mass spectrometry analysis. Chromatography separation was performed using Easy-nLC 1200 (Thermo Fisher Scientific) coupled to an Orbitrap Fusion Lumos mass spectrometer (Thermo Fisher Scientific) using data-dependent mode. Peptides were separated using a 2-30% (v/v) acetonitrile gradient over 80 min, increasing to 45% over the next 5 min, and finally to 95% over 5 min, running at a constant flow rate of 300 nl/min.

The following parameters were set for MS data acquisition: automatic gain control (AGC) customed at normalized target of 100% with orbitrap resolution at 60,000 ranging from m/z 350 to 1550. Dynamic exclusion for precursors selected for fragmentation was set to 90 s. For fragmentation, MS2 isolation window was set to 1.2 m/z of the selected precursor masses and collision-induced dissociation (CID) was activated at 35% normalized collision energy. Fragment signals (MS2) were analysed by an ion trap analyzer set to normal mode, AGC target customed at 150% and maximum injection time (IT) at dynamic mode.

Raw mass spectra were searched using Sequest available in Proteome Discoverer™ (v3.1, Thermo Fisher Scientific) against human primary protein sequences retrieved from uniprot (19 July 2022) with 42289 sequences and 24370425 residues. The mass tolerance for precursors and fragments were set to 20 ppm and 0.8 Da, respectively; and relative quantitation was based on label-free quantitation (LFQ) method.

Phosphoproteomics

Cell pellets were washed with phosphate-buffered saline (PBS) twice and supernatant was removed completely. Samples were then resuspended in 8 M urea in 50 mM 4-(2-hydroxyethyl)-1-piperazineethanesulfonic acid (HEPES), pH 8.0 and sonicated on ice using a probe sonicator at 30-s pulse, 30-s pause for 90 s. Total protein amount was estimated using bicinchoninic acid (BCA) assay and 3 mg proteins from each sample were aliquoted into new tubes. Aliquoted proteins were reduced 10 mM final concentration of tris(2-carboxyethyl)phosphine (TCEP) and incubated for 20 min at 55 °C for disulfide bridge reduction followed by alkylation with 55 mM 2-chloroacetamide (CAA) in the dark for 30 min. The concentration of urea in each sample was reduced to 1 M using 100 mM triethylammonium bicarbonate (TEAB), pH 8.5, then digested with endoproteinase LysC (1:40 enzyme:protein ratio) for 3 h and subsequently by trypsin (1:25 enzyme:protein ratio) at 37 °C overnight. Digestion was terminated by adding 1% (v/v) final concentration of trifluoroacetic acid (TFA) to the samples, followed by desalting using Sep-Pak C18 reversed-phase cartridges. Desalted peptides were separated, where 100 µg of peptides from each sample was taken for whole proteome analysis while the remaining was lyophilized. Lyophilized peptides were resuspended in 6 ml solvent mixture containing 40% (v/v) acetonitrile (ACN) and 6% trifluoroacetic acid (TFA). Phosphopeptide enrichment was carried out by loading the resuspended peptides to 10 mg of titanium dioxide (TiO_2) beads pre-activated using dihydrobenzoic acid. Incubation was performed on a rotator at 25 °C for 10 min. The samples were centrifuged using 1000 × g for 1 min and the supernatant was transferred to a new tube containing 10 mg of TiO_2 beads. Following incubation and centrifugation as described above, the beads were combined in new tubes and washed sequentially with the following buffers: 6% TFA in 10% ACN once; 6% TFA in 40% ACN twice; and finally 6% TFA in 60% ACN twice. Samples were dried by vacuum centrifugation to remove all residual volumes of ACN and TFA.

Phosphopeptides were eluted from the beads by sequential addition and collection of the following buffers: 5% ammonium hydroxide (after 15 min of incubation on a shaker at 25 °C) and 25% ACN in 10% ammonium hydroxide. For each buffer, centrifugation at 14,000 × g was carried out to pellet down the beads and the supernatant was transferred to new tube. Both eluates were combined as a single sample and filtered through a C8 membrane to remove any beads. The membrane was washed with 100% ACN to elute any bound peptides, combined with the initial eluate, and dried by vacuum centrifugation. Dried peptides were washed once using 60% CAN containing 0.1% (v/v) formic acid and re-dried in preparation for mass spectrometry analysis.

Dried fractions were resuspended in 10 µl of 2% (v/v) ACN containing 0.06% (v/v) TFA and 0.5% (v/v) acetic acid and transferred to an autosampler plate. Online chromatography was performed in a Vanquish Neo (Thermo Fisher Scientific) liquid chromatography system using a single-column setup and 0.1% formic acid in water and 0.1% formic acid in 80% acetonitrile asmobile phases. Fractions were injected and separated on a reversed-phase C18 analytical column (Easy-Spray, 75 µm inner diameter × 50 cm length, 2 µm particle size, Thermo Fisher Scientific) maintained at 50 °C and using a 0-35% (v/v) acetonitrile gradient over 60 min, followed by an increase to 50% over the next 8 min, and to 100% over 2 min. The final mixture was maintained on the column for 5 min to elute all remaining peptides. Total run duration for each sample was 75 min at a constant flow rate of 300 nl/min except for the isocratic hold at the final 5 min at 400 nl/min.

Data were acquired using an Orbitrap Eclipse mass spectrometer (Thermo Fisher Scientific) using data-dependent mode. Samples were ionized using 2.1 kV and 300 °C at the nanospray source. Positively-charged precursor signals (MS1) were detected using an Orbitrap analyzer set to 60,000 resolution, automatic gain control (AGC) target of 400,000 ions, and maximum injection time (IT) of 50 ms. Precursors with charges 2-7 within an isolation window of 1.2 m/z of the selected precursor masses and having the highest ion counts in each MS1 scan were further fragmented using collision-induced dissociation (CID) at 35% normalized collision energy. Fragment signals (MS2) were analysed by an ion trap analyzer set to Rapid mode, AGC target of 10,000 and

maximum IT of 35 ms. Precursors used for MS2 scans were excluded for 60 s to avoid re-sampling of high abundance peptides. The MS1–MS2 cycles were repeated every 3 s until completion of the run. Proteins were identified using Proteome Discoverer™ (v3.0, Thermo Fisher Scientific). Raw mass spectra were searched using Sequest against human primary protein sequences retrieved from Swiss-Prot (11 June 2019). Carbamidomethylation on Cys were set as fixed modification; deamidation of asparagine and glutamine, acetylation on protein N-termini, phosphorylation of Ser, Thr, and Tyr residues, and methionine oxidation were set as dynamic modifications for the search. Trypsin/P was set as the digestion enzyme and was allowed up to two missed cleavage sites. Precursors and fragments were accepted if they had a mass error within 20 ppm and 0.8 Da, respectively. Peptides were matched to spectra at a false discovery rate (FDR) of 1% (strict) and5% (relaxed) against the decoy database and quantitated using label-free quantitation (LFQ) method. Search result was exported and further analyzed as described below.

Phosphoproteomics Analysis

Phosphopeptides with at least 2 detectable values out of 3 replicates in at least one group were used for subsequent normalization. Peptides containing valid observations in fewer than 2 replicates were considered as undetected in all 3 samples within this group. The intensity of each phosphopeptide was normalized to the abundance of the corresponding protein. To identify differentially regulated phosphopeptides, missing values were replaced with half of the minimum peptide abundance within each samples, then log 2 (fold changes) and p-values were generated by comparing Opto-PKCε activated group with PMA treated cells. Phosphopeptides with $|\log 2 \text{ (fold changes)}| \geq 1$ and p-value > 0.05, or those only detected in 1 group, were considered as specific phosphorylation events in either Opto-PKCε activation or PMA treatment group. Kinase-Substrate Enrichment Analysis (KSEA) was performed by the R package KSEAapp using default cutoff settings and the annotations from both PhosphoSitePlus and NetworKIN. Kinase Enrichment Analysis (KEA) was conducted by KEA2 webtool.

Molecular Modelling

System setup

The model of human PKCε was obtained from the AlphaFold database[26]. The initial structure for the simulations comprised residues 408–737, which corresponds to the protein kinase domain (residues 408–668) and the C-terminal tail (residues 669-737). A protein BLAST search was conducted on Protein Data Bank (PDB) structures using the FASTA sequence of the region included in our model to identify similar PDB structures containing the ATP ligand and its two associated Mg^{2+} ions bound at the ATP binding site, since they were absent in the AlphaFold model. The highest ranked structure in terms of E-value was the crystal structure of mouse PKA catalytic domain in complex with phospholamban (PDB ID 7E0Z[55]). This structure was aligned to the AlphaFold model of human PKCε before transferring over the ANP and Mg^{2+} to the latter. To convert the ANP to ATP, the nitrogen atom between the beta and gamma phosphate was converted to an oxygen atom. Two systems were set up for simulation, one being T566A mutant PKCε with no C-terminal tail (residues 408–668) and the other being PKCε phosphorylated at Thr566 (residues 408–737). For the system with phosphorylated threonine, the coordinates of phosphorylated threonine were modelled using PyMOL[56].

For each system, the N-terminus of the protein chain was capped with an acetyl group. PDB2PQR[57] was used to determine residue protonation states and add hydrogen atoms. Using the LEaP module of AMBER 22, each system was solvated with TIP3P[58] water molecules in a periodic truncated octahedron box such that the distance between the protein and box edge was at least 10 Å. Sodium counterions were then added to neutralize the systems.

Molecular dynamics (MD) simulations

Energy minimization and MD simulations were performed by the PMEMD module of AMBER22[59] using the ff14SB[60] field for the protein and the generalized AMBER force field (GAFF)[61] for the ATP. Parameters for phosphorylated threonine and ATP were used as described by previous works[62,63]. Bonds involving hydrogen atoms were constrained using the SHAKE[64] algorithm to enable a time step of 2 fs. A nonbonded interaction cutoff distance of 9 Å was used. Long-range electrostatic interactions were treated using the particle mesh Ewald[65] method under periodic boundary conditions. Energy minimization was performed for 500 steps with the steepest descent algorithm, followed by another 500 steps with the conjugate gradient algorithm. The system was then heated gradually to 300 K over 50 ps in the NVT ensemble before equilibration in the NPT ensemble at a constant pressure of 1 atm for another 50 ps. Weak harmonic positional restraints with a force constant of 2.0 kcal mol^{-1} $Å^{-2}$ were imposed on heavy atoms during energy minimization and equilibration steps. Further equilibration without positional restraints was performed for 2 ns, followed by the production run of 500 ns at 300 K and 1 atm. For each system, three simulation runs of conventional molecular dynamics (cMD) simulations with differing initial velocities were performed. The temperature of the system was maintained using a Langevin thermostat[66] with a collision frequency of 2 ps^{-1}, while the pressure was maintained using the Berendsen barostat[67] with a pressure relaxation time of 2 ps.

Accelerated molecular dynamics (aMD) simulations

In aMD, a boost potential ΔV(r) is added to a system's potential energy when the system's potential energy is lower than the threshold energy value E.

$$V(r)^* = V(r) + \Delta V(r), \quad V(r) < E,$$
$$V(r)^* = V(r), \quad V(r) \geq E \tag{1}$$

In this equation above, V(r)* is the modified potential energy, V(r) is the unmodified original potential energy, and ΔV(r) is the boost potential. In the dual-boost implementation of aMD, a boost potential is applied to the system's potential energy and dihedral energy as follows:

$$\Delta V(r) = \frac{\left(E_p - V(r)\right)^2}{\left(\alpha P + E_p - V(r)\right)} + \frac{\left(Ed - Vd(r)\right)^2}{\left(\alpha D + Ed - Vd(r)\right)} \tag{2}$$

In the equation above, E_p is the threshold potential energy, E_d is the threshold dihedral energy, V(r) is the system's potential energy, and Vd(r) is the system's dihedral energy. αP is the acceleration factor for the system's potential energy and αD is the acceleration factor for the system's dihedral energy. The boost parameters were $_{\text{calculated}}$ as follow:

$$\alpha P = 0.2 \times N_{atoms} \tag{3}$$

$$E_p = V_{PE\_avg} + 0.2N_{atoms} \tag{4}$$

$$\alpha D = \frac{4N_{res}}{5} \tag{5}$$

$$Ed = V_{dihed\_avg} + 4N_{res} \tag{6}$$

In the above equations, N_{atoms} is the total number of atoms, N_{res} is the number of protein residues, V_{PE_avg} is the average potential energy and V_{dihed_avg} is the average dihedral energy. V_{PE_avg} and V_{dihed_avg} for aMD were calculated for each system as the average value obtained

from the corresponding 500-ns cMD simulation runs. Dual-boost aMD simulations, in which both dihedral energy and total potential energy are boosted, were initiated from the final structures of each corresponding cMD simulation runs for each system. All aMD simulations were performed at 300 K and 1 atm. Three runs of aMD simulations were performed on each system for 500 ns.

Trajectory analysis

Analysis was performed using the CPPTRAJ[68] module in AMBER22. Hydrogen bond occupancy was calculated using the hbond command. The criteria for hydrogen bond formation are: an acceptor-heavy atom–donor-heavy-atom distance of less than 3.5 Å, and an acceptor heavy atom–donor hydrogen atom–donor heavy atom angle of more than 135º. Hydrogen bond occupancy analysis was performed on the last 400 ns of each simulation run to account for initial equilibration.

AlphaFold3 modeling

Models of monomeric and tetrameric Opto-PKCε were generated using the AlphaFold Server (*http://alphafoldserver.com*), which is based on the AlphaFold3 model[69]. To generate models of the monomer, an amino acid sequence corresponding to Opto-PKCε, 2 ATPs and 1 FAD were used as input whereas for the tetramer, copies of Opto-PKCε, 8 ATPs and 4 FADs were used as input..

Plasmid cloning

CIBN-GFP-CAAX; CRY2high-mCherry (Plasmid #104063) and Flag-PKCε plasmids were purchased from Addgene. For all other plasmids mentioned in this paper, the list of primers is recorded in Table S3. All PCR reactions were done using PhusionFlash High Fidelity Polymerase, followed by Gibson Assembly or InFusion. All plasmids were grown in Stbl3 bacteria and extracted using FavorPrep Plasmid Extraction Kit. Sequences were confirmed using BioBasic Asia Pacific Sequencing Services. Subsequently, amplification and purification were done using Invitrogen™ PureLink™ HiPure Plasmid Filter Maxiprep Kit. Gel-electrophoresis was done to ensure that all synthesized plasmids were clean and of the correct size. Amplified plasmids were stored at −20°C freezer and used for transfection.

Plasmid transient transfection

The day before transfection, HEK293T and HepG2 were split to a density of $2.5*10^6$ cells in 10cm culture dishes and grown in DMEM HG + 10% FBS without P/S media. Cells were transfected using the Expifectamine 293 transfection kit and protocol. For each plate, 20ug of plasmid, 54ul of Expifectamine reagent and 2ml of Opti-MEM were used. No enhancer reagents were added the following day and no media change was carried out unless high cell death was observed. Other than using m199 media instead of DMEM HG, transfection for primary mouse hepatocytes was done in the same way.

Light-delivery system

For light illumination experiments, a 3-by-2 blue LED array was constructed as described in adapted from an earlier report[24]. The array comprises of 24 blue LEDs (LED450L, Thorlabs). The light intensity at the height (12 cm) where the cell culture plate is placed was measured by a power meter (Newark, 1931-C) to be at 200 μW/cm2 with an absolute measurement uncertainty of less than 5%. The working distance of 12-cm is to ensure uniform blue light intensity across the surface of the cell culture dishes.

Optogenetic experiments

Transfected cells were exposed to blue illumination (200 μW/cm^2) using a homemade LED light array while dark plates were kept in the incubator wrapped in aluminium foil. Cell plates exposed to blue light are lysed under ambient light while dark plates are lysed with the aid of red light. For dark recovery, the cells were exposed to blue light before being wrapped in aluminium foil and placed back in the 37°C incubator.

Cells were washed twice with PBS before lysing with 400ul of NP40 lysis buffer supplemented with cOmplete protease inhibitor and PhosSTOP as per manufacturer's instructions.

Plasma membrane and Mitochondria Isolation

Subcellular fractionation of transfected HEK293T and hepatocytes was performed using the Minute™ Plasma Membrane Protein Isolation and Cell Fractionation Kit (Invent Biotechnologies). Steps were followed according to the manual provided.

Co-immunoprecipitation Assay

After cell lysis and protein BCA Assay quantification, samples were diluted to a concentration of 500ug/ml in 500ul using NP40 lysis buffer. Subsequently, 5ul of respective primary antibody was added into each tube and rotated at 4°C overnight before co-immunoprecipitation was carried out as written in the manufacturer's protocol handbook.

Western blot

After lysed samples were agitated at 4°C for 1 hour and centrifuged at 16000g for 20 minutes, supernatant was obtained and quantified using Protein BCA assay on Tecan plate reader. 4X LDS with β-mercaptoethanol buffer was then added to samples and heated at 95°C for 5 minutes before subjecting to electrophoresis using Bio-Rad's MiniPROTEAN system. After separation, protein lanes were transferred onto a nitrocellulose membrane using wet transfer at a constant 300mA for 90 minutes. Membrane was subsequently washed with 0.1% TBS-Triton (TBST) before standard blocking procedure. Primary antibodies used were listed in Key Resource Table.

Fluorescence Microscopy – Live Cell Imaging

35mm glass bottom dishes were coated with 250ul of poly-D-Lysine for 1 hour before rinsing thrice with autoclaved water. COS7 cells were then plated at a density of 0.8*10^5 cells for each dish in DMEM HG media + 10% FBS the day before transfection. 2.5ug of plasmid was transfected using Expifectamine reagent and Opti-MEM as mentioned above and imaging was carried out 24 hours after transfection. To observe the reversibility of Opto-PKCε, images were taken every minute under TRITC filter (557nm, 200ms pulse duration). On the other hand, images were taken every 5 seconds while rotating between FITC (~495nm, 50ms pulse duration) and TRITC (557nm, 200ms pulse duration) filter to observe Opto-PKCε activation. Cells were not continuously shone under the FITC filter to prevent photobleaching. Images were obtained with Nikon Eclipse Ti-E inverted microscope (Nikon Imaging Centre, Singapore), with a CoolSNAP HQ2 CCD Camera, under 100x oil-immersion objective lens (N.A. 1.49).

Immunostaining

COS7 cells were plated at a density of 0.8*10^5 on a 35mm poly-D-lysine coated glass bottom dish and transfected with Opto-PKCε using Expifectamine transfection protocol as mentioned above. Opto-PKCε plate was either treated with continuous blue light for 15 minutes or wrapped with aluminium foil before fixation process. Cells were washed thrice with PBS followed by fixing with 4% PFA for 10 minutes at room temperature. Following that, cells were washed thrice with PBS and incubated in permeabilization solution for 5 minutes. This is followed by blocking using 10%

FBS in PBS for 1.5 hours in a 37°C incubator. Cells were then stained with primary antibodies for 1 hour. After washing thrice with PBS, cells were then incubated with secondary antibody (Alexa Fluor 488, 1:300) and wrapped in aluminium foil for 1 hour. Detailed information regarding 1st and 2nd antibodies was provided in the Key Resources Table. Images were taken using a conventional fluorescence microscope with an oil-immersion 100x objective lens.

Seahorse XF Cell Mito Stress Assay

Reagents and apparatus used to perform Seahorse XF Cell Mito Stress Test Kit were all purchased from Agilent. 24 well seahorse culture plates were first coated with poly-D-lysine and incubated in 37°C incubator containing 5% CO2 for 1 hour before washing twice with PBS. Rows C and D were wrapped with aluminium foil and secured with aluminium tape. Plate covers were also covered in aluminium tape to prevent exposure of blue light to the cells. Plates and covers were treated with UV for 30 mins in the culture hood before transfected HEK293T cells were seeded at 0.4*10^5 cells per well in DMEM HG + 10%FBS + 1% P/S. 18 hours after seeding, cells were incubated in the Seahorse XF DMEM Medium supplemented with 10Mm glucose and 2mm sodium pyruvate for 45mins in a 37°C incubator with no CO2. Media change was performed in the dark. Cells were subsequently exposed to 15mins of blue light and loaded into the seahorse machine probe. Probes were incubated in calibrant overnight before the experiment. 4um of Oligomycin, 0.5um of FCCP, 1um of Antimycin A and Rotenone were injected into the cells at different time points preset on the machine and OCR response was recorded.

Quantification

All quantifications were done using Image J, Graph analysis was done using GraphPad Prism Software 8.4.3.

Data availability statement

The data are available from the corresponding author upon reasonable request

Acknowledgements

This work was supported by the A*STAR Biomedical Research Council core fund, A*STAR Strategic Research Program (the Brain-Body Initiative, iGrants call ID #21718), A*STAR Use-Inspired Basic Research Award to W.H. Q.O. gratefully acknowledges support from the NMRC (National Medical Research Council) YIRG grant (OFYIRG19nov-0045). X.Y. was supported by grants from National Institutes of Health (R01DK089098, R01DK102648, R01DK137467). G.I.S. was supported by grants from the US Public Health Services NIH/NIDDK (R01 DK133143 and P30 DK045735). J.T.N. and Y.S.T. are supported by the Bioinformatics Institute, A*STAR and A*STAR's BMRC Central Research Fund award. We would like to thank Dr. Xiao-Bing Gao and Prof Bianxiao Cui for their feedback and comments.

Additional information

Author contributions

Conceptualization - Q.O.

Methodology - Q.O., R.M.S., Y.S.T., G.I.S. and W.H.

Data curation and investigation - Q.O., C.J.Y.L., L.T.R.L., S.K., S.E.C., P.L.Y.Y., H.L., J.T.N., L.C.W. and S.G.L.

Formal analysis - Q.O., C.J.Y.L., Y.L., J.T.N. and Y.S.T. analyzed the data.

Writing original draft – Q.O. and C.L.

Writing: review and editing - Q.O., Y.S.T, X.Y. and W.H.

Additional files

Supplementary material. *Figures S1-S6 and Table S4.*

Table S1.

Table S2.

Table S3.

Data S1.

References

1. Sen A., Nelson T.J., Alkon D.L., Hongpaisan J. (2018) **Loss in PKC Epsilon Causes Downregulation of MnSOD and BDNF Expression in Neurons of Alzheimer's Disease Hippocampus** *J Alzheimers Dis* **63**:1173–1189 https://doi.org/10.3233/JAD-171008

2. Chen Y., Tian Q. (2011) **The role of protein kinase C epsilon in neural signal transduction and neurogenic diseases** *Front Med* **5**:70–76 https://doi.org/10.1007/S11684-011-0119-9

3. Nelson T.J., Sun M.K., Lim C., Sen A., Khan T., Chirila F. V., Alkon D.L. (2017) **Bryostatin Effects on Cognitive Function and PKCε in Alzheimer's Disease Phase IIa and Expanded Access Trials** *J Alzheimers Dis* **58**:521–535 https://doi.org/10.3233/JAD-170161

4. Hongpaisan J., Sun M.K., Alkon D.L. (2011) **PKC ε Activation Prevents Synaptic Loss, Aβ Elevation, and Cognitive Deficits in Alzheimer's Disease Transgenic Mice** *Journal of Neuroscience* **31**:630–643 https://doi.org/10.1523/JNEUROSCI.5209-10.2011

5. He S., Li Q., Huang Q., Cheng J. (2022) **Targeting Protein Kinase C for Cancer Therapy** *Cancers 2022, Vol. 14, Page 1104* **14**:1104 https://doi.org/10.3390/CANCERS14051104

6. Nowak G., Bakajsova D., Samarel A.M. (2011) **Protein kinase C-ε activation induces mitochondrial dysfunction and fragmentation in renal proximal tubules** *Am J Physiol Renal Physiol* **301**:F197 https://doi.org/10.1152/AJPRENAL.00364.2010

7. Dehghani H., Reith C., Hahnel A.C. (2005) **Subcellular localization of protein kinase C δ and ε affects transcriptional and post-transcriptional processes in four-cell mouse embryos** *Reproduction* **130**:453–465 https://doi.org/10.1530/REP.1.00572

8. Keenan C., Volkov Y., Kelleher D., Long A. (1997) **Subcellular localization and translocation of protein kinase C isoforms zeta and epsilon in human peripheral blood lymphocytes** *Int Immunol* **9**:1431–1439 https://doi.org/10.1093/INTIMM/9.10.1431

9. Goodnight J., Mischak H., Kolch W., Mushinski J.F. (1995) **Immunocytochemical localization of eight protein kinase C isozymes overexpressed in NIH 3T3 fibroblasts. Isoform-specific association with microfilaments, Golgi, endoplasmic reticulum, and nuclear and cell membranes** *J Biol Chem* **270**:9991–10001 https://doi.org/10.1074/JBC.270.17.9991

10. Lehel C., Olah Z., Jakab G., Anderson W.B. (1995) **Protein kinase C epsilon is localized to the Golgi via its zinc-finger domain and modulates Golgi function** *Proc Natl Acad Sci U S A* **92**:1406 https://doi.org/10.1073/PNAS.92.5.1406

11. Duquesnes N., Lezoualc'h F., Crozatier B. (2011) **PKC-delta and PKC-epsilon: Foes of the same family or strangers?** *J Mol Cell Cardiol* **51**:665–673 https://doi.org/10.1016/J.YJMCC.2011.07.013

12. Summanen M., Granqvist N., Tuominen R.K., Yliperttula M., Verrips C.T., Boonstra J., Blanchetot C., Ekokoski E. (2012) **Kinetics of PKCε Activating and Inhibiting Llama Single Chain Antibodies and Their Effect on PKCε Translocation in HeLa Cells** *PLoS One* **7**:35630 https://doi.org/10.1371/JOURNAL.PONE.0035630

13. Mukherjee A., Roy S., Saha B., Mukherjee D. (2016) **Spatio-temporal regulation of PKC isoforms imparts signaling specificity** *Front Immunol* **7**:45 https://doi.org/10.3389/FIMMU.2016.00045/BIBTEX

14. Liu M., Idkowiak-Baldys J., Roddy P.L., Baldys A., Raymond J., Clarke C.J., Hannun Y.A. (2013) **Sustained Activation of Protein Kinase C Induces Delayed Phosphorylation and Regulates the Fate of Epidermal Growth Factor Receptor** *PLoS One* **8**:e80721 https://doi.org/10.1371/JOURNAL.PONE.0080721

15. Xu Y., Nan D., Fan J., Bogan J.S., Toomre D. (2016) **Optogenetic activation reveals distinct roles of PI(3,4,5)P3 and Akt in adipocyte insulin action** *J Cell Sci* **129**:2085–2095 https://doi.org/10.1242/jcs.174805

16. Katsura Y., Kubota H., Kunida K., Kanno A., Kuroda S., Ozawa T. (2015) **An optogenetic system for interrogating the temporal dynamics of Akt** *Sci Rep* **5**:14589 https://doi.org/10.1038/srep14589

17. Wend S., Wagner H.J., Müller K., Zurbriggen M.D., Weber W., Radziwill G. (2014) **Optogenetic Control of Protein Kinase Activity in Mammalian Cells** *ACS Synth Biol* **3**:280–285 https://doi.org/10.1021/sb400090s

18. Duan L., Hope J.M., Guo S., Ong Q., François A., Kaplan L., Scherrer G., Cui B. (2018) **Optical Activation of TrkA Signaling** *ACS Synth Biol* **7**:1685–1693 https://doi.org/10.1021/acssynbio.8b00126

19. Cenni V., Döppler H., Sonnenburg E.D., Maraldi N., Newton A.C., Toker A. (2002) **Regulation of novel protein kinase C epsilon by phosphorylation** *Biochemical Journal* **363**:537 https://doi.org/10.1042/0264-6021:3630537

20. Swanson C.J., Sommese R.F., Petersen K.J., Ritt M., Karslake J., Thomas D.D., Sivaramakrishnan S. (2016) **Calcium Stimulates Self-Assembly of Protein Kinase C α In Vitro** *PLoS One* **11**:e0162331 https://doi.org/10.1371/JOURNAL.PONE.0162331

21. Swanson C.J., Ritt M., Wang W., Lang M.J., Narayan A., Tesmer J.J., Westfall M., Sivaramakrishnan S. (2014) **Conserved modular domains team up to latch-open active protein kinase Cα** *Journal of Biological Chemistry* **289**:17812–17829 https://doi.org/10.1074/jbc.M113.534750

22. Bonny M., Hui X., Schweizer J., Kaestner L., Zeug A., Kruse K., Lipp P. (2016) **C2-domain mediated nano-cluster formation increases calcium signaling efficiency** *Scientific Reports 2016 6:1* **6**:1–11 https://doi.org/10.1038/srep36028

23. Idevall-Hagren O., Dickson E.J., Hille B., Toomre D.K., De Camilli P. (2012) **Optogenetic control of phosphoinositide metabolism** *Proc Natl Acad Sci U S A* **109**:E2316–23 https://doi.org/10.1073/pnas.1211305109

24. Zhang K., Duan L., Ong Q., Lin Z., Varman P.M., Sung K., Cui B. (2014) **Light-mediated kinetic control reveals the temporal effect of the Raf/MEK/ERK pathway in PC12 cell neurite outgrowth** *PLoS One* **9**

25. Ong Q., Guo S., Duan L., Zhang K., Collier E.A., Cui B. (2016) **The Timing of Raf/ERK and AKT Activation in Protecting PC12 Cells against Oxidative Stress** *PLoS One* **11**:e0153487 https://doi.org/10.1371/journal.pone.0153487

26. Jumper J., Evans R., Pritzel A., Green T., Figurnov M., Ronneberger O., Tunyasuvunakool K., Bates R., Žídek A., Potapenko A., et al. (2021) **Highly accurate protein structure prediction with AlphaFold** *Nature* **596**:583–589 https://doi.org/10.1038/S41586-021-03819-2

27. Heemskerk F.M.J., Chen H.C., Huang F.L. (1993) **Protein kinase C phosphorylates Ser152, Ser156 and Ser163 but not Ser160 of MARCKS in rat brain** *Biochem Biophys Res Commun* **190**:236–241 https://doi.org/10.1006/BBRC.1993.1036

28. Wiredja D.D., Koyutürk M., Chance M.R. (2017) **The KSEA App: a web-based tool for kinase activity inference from quantitative phosphoproteomics** *Bioinformatics* **33**:3489–3491 https://doi.org/10.1093/BIOINFORMATICS/BTX415

29. Lachmann A., Ma'ayan A. (2009) **KEA: kinase enrichment analysis** *Bioinformatics* **25**:684–686 https://doi.org/10.1093/BIOINFORMATICS/BTP026

30. Jabůrek M., Costa A.D.T., Burton J.R., Costa C.L., Garlid K.D. (2006) **Mitochondrial PKCε and Mitochondrial ATP-Sensitive K+ Channel Copurify and Coreconstitute to Form a Functioning Signaling Module in Proteoliposomes** *Circ Res* **99**:878–883 https://doi.org/10.1161/01.RES.0000245106.80628.D3

31. Morris-Blanco K.C., Dave K.R., Saul I., Koronowski K.B., Stradecki H.M., Perez-Pinzon M.A. (2016) **Protein Kinase C Epsilon Promotes Cerebral Ischemic Tolerance Via Modulation of Mitochondrial Sirt5** *Scientific Reports 2016 6:1* **6**:1–15 https://doi.org/10.1038/srep29790

32. Kennedy M.J., Hughes R.M., Peteya L.A., Schwartz J.W., Ehlers M.D., Tucker C.L. (2010) **Rapid blue-light-mediated induction of protein interactions in living cells** *Nat Methods* **7**:973–975 https://doi.org/10.1038/nmeth.1524

33. Petersen M.C., Madiraju A.K., Gassaway B.M., Marcel M., Nasiri A.R., Butrico G., Marcucci M.J., Zhang D., Abulizi A., Zhang X.M., et al. (2016) **Insulin receptor Thr1160 phosphorylation mediates lipid-induced hepatic insulin resistance** *J Clin Invest* **126**:4361–4371 https://doi.org/10.1172/JCI86013

34. Lyu K., Zhang Y., Zhang D., Kahn M., ter Horst K.W., Rodrigues M.R.S., Gaspar R.C., Hirabara S.M., Luukkonen P.K., Lee S., et al. (2020) **A Membrane-Bound Diacylglycerol Species Induces PKCε-Mediated Hepatic Insulin Resistance** *Cell Metab* **32**:654–664 https://doi.org/10.1016/J.CMET.2020.08.001

35. Brandon A.E., Liao B.M., Diakanastasis B., Parker B.L., Raddatz K., McManus S.A., O'Reilly L., Kimber E., van der Kraan A.G., Hancock D., et al. (2019) **Protein Kinase C Epsilon Deletion in Adipose Tissue, but Not in Liver, Improves Glucose Tolerance** *Cell Metab* **29**:183–191 https://doi.org/10.1016/j.cmet.2018.09.013

36. Johnson J.L., Yaron T.M., Huntsman E.M., Kerelsky A., Song J., Regev A., Lin T.Y., Liberatore K., Cizin D.M., Cohen B.M., et al. (2023) **An atlas of substrate specificities for the human serine/threonine kinome** *Nature 2023 613:7945* **613**:759–766 https://doi.org/10.1038/s41586-022-05575-3

37. Cooke M., Magimaidas A., Casado-Medrano V., Kazanietz M.G. (2017) **Protein kinase C in cancer: The top five unanswered questions** *Mol Carcinog* **56**:1531–1542 https://doi.org/10.1002/MC.22617

38. Toettcher J.E., Weiner O.D., Lim W.A. (2013) **Using optogenetics to interrogate the dynamic control of signal transmission by the Ras/Erk module** *Cell* **155**:1422–1434 https://doi.org/10

.1016/j.cell.2013.11.004

39. Hughes R.M., Freeman D.J., Lamb K.N., Pollet R.M., Smith W.J., Lawrence D.S. (2015) **Optogenetic Apoptosis: Light-Triggered Cell Death** *Angewandte Chemie International Edition* **54**:12064–12068 https://doi.org/10.1002/ANIE.201506346

40. Wang X., He L., Wu Y.I., Hahn K.M., Montell D.J. (2010) **Light-mediated activation reveals a key role for Rac in collective guidance of cell movement in vivo** *Nat Cell Biol* **12**:591–597 https://doi.org/10.1038/ncb2061

41. Wu Y.I., Frey D., Lungu O.I., Jaehrig A., Schlichting I., Kuhlman B., Hahn K.M. (2009) **A genetically encoded photoactivatable Rac controls the motility of living cells** *Nature 2009 461:7260* **461**:104–108 https://doi.org/10.1038/nature08241

42. Gada K.D., Kawano T., Plant L.D., Logothetis D.E. (2022) **An optogenetic tool to recruit individual PKC isozymes to the cell surface and promote specific phosphorylation of membrane proteins** *Journal of Biological Chemistry* **298**:101893 https://doi.org/10.1016/J.JBC.2022.101893

43. Xu T.R., Rumsby M.G. (2004) **Phorbol ester-induced translocation of PKC epsilon to the nucleus in fibroblasts: Identification of nuclear PKC epsilon-associating proteins** *FEBS Lett* **570**:20–24 https://doi.org/10.1016/j.febslet.2004.05.080

44. O'Banion C.P., Priestman M.A., Hughes R.M., Herring L.E., Capuzzi S.J., Lawrence D.S. (2018) **Design and Profiling of a Subcellular Targeted Optogenetic cAMP-Dependent Protein Kinase** *Cell Chem Biol* **25**:100 https://doi.org/10.1016/J.CHEMBIOL.2017.09.011

45. Newton A.C. (2018) **Protein Kinase C: Perfectly Balanced** *Crit Rev Biochem Mol Biol* **53**:208 https://doi.org/10.1080/10409238.2018.1442408

46. Cacace A.M., Ueffing M., Philipp A., Han E.K.H., Kolch W., Weinstein I.B. (1996) **PKC epsilon functions as an oncogene by enhancing activation of the Raf kinase** *Oncogene* **13**:2517–2526

47. Ueffing M., Lovrić J., Philipp A., Mischak H., Kolch W. (1997) **Protein kinase C-epsilon associates with the Raf-1 kinase and induces the production of growth factors that stimulate Raf-1 activity** *Oncogene* **15**:2921–2927 https://doi.org/10.1038/SJ.ONC.1201477

48. Galeotti N., Ghelardini C. (2012) **Selective modulation of the PKCε/p38MAP kinase signalling pathway for the antidepressant-like activity of amitriptyline** *Neuropharmacology* **62**:289–296 https://doi.org/10.1016/J.NEUROPHARM.2011.07.020

49. Kabir N., Schaefer A.W., Nakhost A., Sossin W.S., Forscher P. (2001) **Protein Kinase C Activation Promotes Microtubule Advance in Neuronal Growth Cones by Increasing Average Microtubule Growth Lifetimes** *J Cell Biol* **152**:1033 https://doi.org/10.1083/JCB.152.5.1033

50. Steinberg S.F. (2008) **Structural Basis of Protein Kinase C Isoform Function** *Physiol Rev* **88**:1341 https://doi.org/10.1152/PHYSREV.00034.2007

51. Kumashiro N., Erion D.M., Zhang D., Kahn M., Beddow S.A., Chu X., Still C.D., Gerhard G.S., Han X., Dziura J., et al. (2011) **Cellular mechanism of insulin resistance in nonalcoholic fatty liver disease** *Proc Natl Acad Sci U S A* **108**:16381–16385 https://doi.org/10.1073/PNAS.1113359108

52. Nowak G., Takacsova-Bakajsova D., Megyesi J. (2017) **Deletion of protein kinase C-ε attenuates mitochondrial dysfunction and ameliorates ischemic renal injury** *Am J Physiol Renal Physiol* **312**:F109–F120 https://doi.org/10.1152/AJPRENAL.00115.2016/ASSET/IMAGES/LARGE/ZH20161680850008.JPEG

53. Jain K., Basu A. (2014) **The Multifunctional Protein Kinase C-ε in Cancer Development and Progression** *Cancers 2014, Vol. 6, Pages 860-878* **6**:860–878 https://doi.org/10.3390/CANCERS6020860

54. Zisopoulou S., Asimaki O., Leondaritis G., Vasilaki A., Sakellaridis N., Pitsikas N., Mangoura D. (2013) **PKC-epsilon activation is required for recognition memory in the rat** *Behavioural brain research* **253**:280–289 https://doi.org/10.1016/J.BBR.2013.07.036

55. Qin J., Zhang J., Lin L., Haji-Ghassemi O., Lin Z., Woycechowsky K.J., Van Petegem F., Zhang Y., Yuchi Z. (2022) **Structures of PKA–phospholamban complexes reveal a mechanism of familial dilated cardiomyopathy** *eLife* **11** https://doi.org/10.7554/ELIFE.75346

56. DeLano W.L. (2002) **The PyMOL Molecular Graphics System**

57. Dolinsky T.J., Nielsen J.E., McCammon J.A., Baker N.A. (2004) **PDB2PQR: an automated pipeline for the setup of Poisson–Boltzmann electrostatics calculations** *Nucleic Acids Res* **32**:W665–W667 https://doi.org/10.1093/NAR/GKH381

58. Jorgensen W.L., Chandrasekhar J., Madura J.D., Impey R.W., Klein M.L. (1983) **Comparison of simple potential functions for simulating liquid water** *J Chem Phys* **79**:926–935 https://doi.org/10.1063/1.445869

59. Case D.A., Aktulga H.M., Belfon K., Ben-Shalom I.Y., Berryman J.T., Brozell S.R., Cerutti D.S., Cheatham T.E., Cisneros G.A., Cruzeiro V.W.D., et al. (2022) **AMBER 22** San Francisco: University of California

60. Maier J.A., Martinez C., Kasavajhala K., Wickstrom L., Hauser K.E., Simmerling C. (2015) **ff14SB: Improving the Accuracy of Protein Side Chain and Backbone Parameters from ff99SB** *J Chem Theory Comput* **11**:3696–3713 https://doi.org/10.1021/ACS.JCTC.5B00255/SUPPL_FILE/CT5B00255_SI_001.PDF

61. Wang J., Wolf R.M., Caldwell J.W., Kollman P.A., Case D.A. (2004) **Development and testing of a general amber force field** *J Comput Chem* **25**:1157–1174 https://doi.org/10.1002/JCC.20035

62. Meagher K.L., Redman L.T., Carlson H.A. (2003) **Development of polyphosphate parameters for use with the AMBER force field** *J Comput Chem* **24**:1016–1025 https://doi.org/10.1002/JCC.10262

63. Homeyer N., Horn A.H.C., Lanig H., Sticht H. (2006) **AMBER force-field parameters for phosphorylated amino acids in different protonation states: phosphoserine, phosphothreonine, phosphotyrosine, and phosphohistidine** *J Mol Model* **12**:281–289 https://doi.org/10.1007/S00894-005-0028-4

64. Ryckaert J.P., Ciccotti G., Berendsen H.J.C. (1977) **Numerical integration of the cartesian equations of motion of a system with constraints: molecular dynamics of n-alkanes** *J Comput Phys* **23**:327–341 https://doi.org/10.1016/0021-9991(77)90098-5

65. Darden T., York D., Pedersen L. (1993) **Particle mesh Ewald: An N⋅log(N) method for Ewald sums in large systems** *J Chem Phys* **98**:5648 https://doi.org/10.1063/1.464397

66. Lzaguirre J.A., Catarello D.P., Wozniak J.M., Skeel R.D. (2001) **Langevin stabilization of molecular dynamics** *J Chem Phys* **114**:2090–2098 https://doi.org/10.1063/1.1332996

67. Berendsen H.J.C., Postma J.P.M., Van Gunsteren W.F., Dinola A., Haak J.R. (1984) **Molecular dynamics with coupling to an external bath** *J Chem Phys* **81**:3684–3690 https://doi.org/10.1063/1.448118

68. Roe D.R., Cheatham T.E. (2013) **PTRAJ and CPPTRAJ: Software for processing and analysis of molecular dynamics trajectory data** *J Chem Theory Comput* **9**:3084–3095 https://doi.org/10.1021/CT400341P/SUPPL_FILE/CT400341P_SI_001.PDF

69. Abramson J., Adler J., Dunger J., Evans R., Green T., Pritzel A., Ronneberger O., Willmore L., Ballard A.J., Bambrick J., et al. (2024) **Accurate structure prediction of biomolecular interactions with AlphaFold 3** *Nature 2024 630:8016* **630**:493–500 https://doi.org/10.1038/s41586-024-07487-w

Author information

Qunxiang Ong[*†]
Laboratory of Metabolic Medicine, Institute of Molecular and Cell Biology, Agency for Science, Technology and Research (A*STAR), Singapore, Singapore
ORCID iD: 0000-0003-3674-2105

For correspondence: ongqx@imcb.a-star.edu.sg
[*]These authors contributed equally.
[†]Lead contact.

Crystal Jing Yi Lim[*]
Laboratory of Metabolic Medicine, Institute of Molecular and Cell Biology, Agency for Science, Technology and Research (A*STAR), Singapore, Singapore

[*]These authors contributed equally.

Yilie Liao
Laboratory of Metabolic Medicine, Institute of Molecular and Cell Biology, Agency for Science, Technology and Research (A*STAR), Singapore, Singapore, Duke-NUS Medical School, National University of Singapore, Singapore, Singapore

Justin Tze-Yang Ng
Bioinformatics Institute, Agency for Science, Technology and Research (A*STAR), Singapore, Singapore

Ler Ting Rachel Lim
Laboratory of Metabolic Medicine, Institute of Molecular and Cell Biology, Agency for Science, Technology and Research (A*STAR), Singapore, Singapore

Shernys Xuan Yi Koh
Laboratory of Metabolic Medicine, Institute of Molecular and Cell Biology, Agency for Science, Technology and Research (A*STAR), Singapore, Singapore

Sher En Chan
Laboratory of Metabolic Medicine, Institute of Molecular and Cell Biology, Agency for Science, Technology and Research (A*STAR), Singapore, Singapore

Pheobe Lee Yu Ying
Laboratory of Metabolic Medicine, Institute of Molecular and Cell Biology, Agency for Science, Technology and Research (A*STAR), Singapore, Singapore

Huijun Lim
Laboratory of Metabolic Medicine, Institute of Molecular and Cell Biology, Agency for Science, Technology and Research (A*STAR), Singapore, Singapore

Chen Rui Ye
Laboratory of Metabolic Medicine, Institute of Molecular and Cell Biology, Agency for Science, Technology and Research (A*STAR), Singapore, Singapore

Loo Chien Wang
Functional Proteomics Laboratory, SingMass National Laboratory, Institute of Molecular and Cell Biology, Agency for Science, Technology and Research (A*STAR), Singapore, Singapore

Siok Ghee Ler
Functional Proteomics Laboratory, SingMass National Laboratory, Institute of Molecular and Cell Biology, Agency for Science, Technology and Research (A*STAR), Singapore, Singapore

Radoslaw M Sobota
Functional Proteomics Laboratory, SingMass National Laboratory, Institute of Molecular and Cell Biology, Agency for Science, Technology and Research (A*STAR), Singapore, Singapore

Yaw Sing Tan
Bioinformatics Institute, Agency for Science, Technology and Research (A*STAR), Singapore, Singapore

Gerald I Shulman
Departments of Internal Medicine and Cellular & Molecular Physiology, Yale School of Medicine, New Haven, United States, Howard Hughes Medical Institute, Chevy Chase, United States

Xiaoyong Yang
Departments of Comparative Medicine and Cellular & Molecular Physiology, Yale School of Medicine, New Haven, United States

Weiping Han
Laboratory of Metabolic Medicine, Institute of Molecular and Cell Biology, Agency for Science, Technology and Research (A*STAR), Singapore, Singapore

For correspondence: hanw@imcb.a-star.edu.sg

Editors

Reviewing Editor
Alejandro San Martín
Centro de Estudios Científicos and Universidad San Sebastián, Valdivia, Chile

Senior Editor
Qiang Cui
Boston University, Boston, United States of America

Reviewer #1 (Public review):

Summary:

Optogenetic tools enable very precise spatiotemporal control of the signaling pathway. The authors developed an optimized light-regulated PKC epsilon, Opto-PKCepsilon using AlphaFold for rational design. Interactome and phosphoproteome studies of light-activated Opto-PKCepsilon confirmed a high similarity of interaction partners to PMA-stimulated wild-type PKCepsilon and high specificity for PKCepsilon substrates. Light-dependent recruitment of Opto-PKCepsilon to the plasma membrane revealed the specific phosphorylation of the insulin receptor at Thr 1160 and recruitment to mitochondria the phosphorylation of the complex I subunit NDUFS4 correlating with reduced spare respiratory capacity, respectively. The interactome and phosphoproteome studies confirm the functionality of Opto-PKCepsilon.

Strengths:

AlphaFold simulations enable the design of an optimized Opto-PKCepsilon with respect to dark-light activity. Opto-PKCepsilon is a versatile tool to study the function of PKCepsilon in a precisely controlled manner.

Weaknesses:

Light-controlled PCKepsilon was recently reported by Gada et al. (2022). Ong et al. developed an optimized Opto-PKCepsilon and presented in their manuscript the potential of this tool for controlling signaling pathways. However, some data have to be improved and appropriate controls are still missing for some experiments.

Major comments:

(1) The group of proteins detected as phosphorylated PKC substrates (phospho-Ser PKC substrate antibody) induced by Opto-PKCepsilon varies significantly between Figure 1 C and Figure 2 C. Have the authors any explanation for this? Do both figures show similar areas of the membrane? The size marker indicates that this is not the case.

(2) The ratio of endogenous and exogeneous PCKepsilon is quite different in the experiments shown in Figure 1 C and Figure 2 C. What is the reason for this effect?

(3) In addition to the overall phosphorylation of PKC substrates, the PKCepsilon mutants should be tested for phosphorylation of a known PKCepsilon substrate. The phosphorylation of the insulin receptor at Thr 1160 by Opto-PKCepsilon (see Figure 6) is very convincing and would provide clearer results for comparing the mutants.

(4) The quality of the fluorescence images shown in Figure 5 is poor and should be improved. In addition, a MitoTracker dye for mitochondria labeling should be included to confirm the mitochondrial localization of Opto-PKCepsilon.

(5) Figure S6 shows a light experiment in the absence of insulin, as stated in the headline of the figure legend and in the main text. Does this mean that Figure 6B shows an experiment in which the cells were exposed to light in the presence of insulin? If so, this should be mentioned in the legend of the figure and in the main text. What influence does insulin have on IR phosphorylation at Thr 1160?

(6) The signal of NDUSF4 phosphorylation induced by Opto-PKCepsilon is weak in the experiment shown in Figure 7E. What about the effect of shorter and longer exposure times? How many times was this experiment repeated?

https://doi.org/10.7554/eLife.105796.1.sa1

Reviewer #2 (Public review):

Summary:

The authors developed an optogenetic tool (Opto-PKCε) and demonstrated spatiotemporal control of optoPKCε at different subcellular compartments such as the plasma membrane or mitochondria. Signaling outcomes of optoPKCε were characterized by phosphoproteomics and biochemical analysis of downstream signaling effectors.

Strengths:

(1) Conventional strategy to activate PKC often involves activation of multiple downstream signaling pathways. This work showcases an alternative strategy that could help dissect the effect of specific PKC-elicited signaling outcomes.

(2) The differential phosphoproteomic analysis of PKC substrates between PMA stimulation and optoPKCε activation is insightful. A follow-up question is whether co-transfection of CIBN-GFP-CaaX and optoPKCε increases the pool of substrate compared to optoPKCε only, or optoPKCε activation at the plasma membrane is more effective in phosphorylating its substrates?

(3) The finding that PKC activation at the plasma membrane is required for insulin receptor activation is interesting. Why does Thr1160 phosphorylation lead to a reduction of Thr1158/1162/1163? Does "insulin-stimulated" imply that insulin was administrated in the culture during optogenetic stimulation? Also, did the author observe any insulin receptor endocytosis upon optoPKCε activation?

Weaknesses:

(1) When citing the previous work on optogenetics, the reviewer believes a broader scope of papers (reviews) and recent research articles should be cited, especially those that used similar strategies, i.e., membrane translocation followed by oligomerization (of cryptochrome), as reported in this work.

(2) In terms of molecular modeling, how would the author enable AlphaFold3 structure prediction of activated optoPKCε (or the blue-light stimulated state of cryptochrome)? Current methods only describe that "To generate models of the monomer, an amino acid sequence corresponding to Opto-PKCε, 2 ATPs and 1 FAD were used as input whereas for the tetramer, copies of Opto-PKCε, 8 ATPs and 4 FADs were used as input" (likely missing "four" between "tetramer" and "copies"). However, simply putting four monomers would not ensure that each monomer is in the "activated" state, which involves excitation of the FAD cofactor and likely conformational changes in cryptochrome.

(3) It would be helpful if the authors could help interpret some results. For example, Figure S1: Was the puncta of mCherry-PKCε on the plasma membrane or within the cytosol? Also, why does optoPKCε only work when PKCε is fused at the C-terminus? When screening for the optoPKCε system with the largest light-to-dark contrast, the AGC domain was truncated. What is the physiological function of AGC? Does AGC removal limit PKC's access to its endogenous substrates?

https://doi.org/10.7554/eLife.105796.1.sa0